Energy & Buildings 261 (2022) 111944

Contents lists available at ScienceDirect

Energy & Buildings

journal homepage: www.elsevier.com/locate/enb

Predictive control of multi-zone variable air volume air-conditioning system based on radial basis function neural network

Lei Lei [a], Wei Liu [b,*]

[a] School of Civil Engineering and Architecture, Zhejiang Sci-Tech University, Hangzhou 310018, China
[b] Division of Sustainable Buildings, Department of Civil and Architectural Engineering, KTH Royal Institute of Technology, Brinellvägen 23, Stockholm 10044, Sweden

ARTICLE INFO

Article history:
Received 9 December 2021
Revised 23 January 2022
Accepted 10 February 2022
Available online 14 February 2022

Keywords:
Multi-zone building
Air-conditioning system
VAV
RBF neural network
Predictive control

ABSTRACT

The multi-zone variable air volume (VAV) air-conditioning system is a complex thermal system with large delay and nonlinearity. Due to the complex environment of multi-zone buildings and the complicated operation process of the VAV air-conditioning system, there are many difficulties in the room temperature control. This paper firstly establishes a multi-zone building model for room temperature using resistance–capacitance method. This investigation simulates and measures the dynamic response of room temperature in a three-floor building without/with air-conditioning for validation. Then a multi-zone VAV air-conditioning system room temperature predictive control model based on radial basis function (RBF) neural network (NN) is proposed. This study sets up a multi-zone VAV air-conditioning system experimental platform in the three rooms on the first floor of the building and implements the predictive control model based on the RBF neural network. The experimental results show that the predictive control model based on RBF NN is able to meet room temperature requirements. It also has strong anti-interference performance and ensures stable static pressure of the main air supply duct. The multi-zone building model can accurately simulate the temperature changes of each room when the air supply volume varies.

1. Introduction

Air-conditioning system is typically used to remove/supply heat and moisture from/to the built environment for ensuring the occupants' thermal comfort. In terms of ventilation rates, the traditional air-conditioning system supplies constant air volume (CAV) and chilled water in disregard of the changes in heating/cooling load, which inevitably leads to waste of energy. In order to obtain higher energy-efficiency and a better indoor climate, variable air volume (VAV) air-conditioning and demand control ventilation (DCV) is widely used in offices and commercial buildings. VAV and DCV systems are able to adjust the ventilation and air conditioning in response to varying activity levels [1]. Comparing with the CAV system, the VAV/DCV systems has more precise temperature control, reduced compressor wear, lower energy consumption by system fans, less fan noise, and additional passive dehumidification [2,3]. VAV air-conditioning system uses the most basic demand control and allows the air flow to be adjusted in response to factors such as temperature or air quality. DCV system uses advanced demand control and adjusts the air flow and temperature in response to demand and occupancy status in rooms. A VAV air-conditioning system is not as advanced as a DCV system, but it generally has lower investment cost and would be perfectly adequate for projects with less advanced demand scenario or construction sites with little intermittent change in the flow of people.

Room temperature control is the core and foundation of the VAV system. Accurate room temperature control can improve the performance of the VAV air-conditioning system, so the requirements for control accuracy are getting higher and higher. The room temperature depends on the building envelope, indoor heat source, outdoor environment, and the operation of the VAV terminal. Therefore, a multi-zone building mathematical model that can predict the dynamic response of room temperature need to be established to accurately control the room temperature of the multi-zone VAV air-conditioning system. In the study of multi-zone building models, some researchers use resistance–capacitance (RC) network methods to simplify the building envelope model and establish a multi-zone mathematical model to simulate room temperature changes under different working conditions [4–6]. Jin et al., [7] used the heat capacity and thermal resistance network method to divide the wall and other building envelope into one-layer structure and established a multi-zone mathematical model of air-conditioning in a room with partition walls. Although the

* Corresponding author.
E-mail address: weiliu2@kth.se (W. Liu).

https://doi.org/10.1016/j.enbuild.2022.111944
0378-7788/

Nomenclature

A_{la}	contact area between the work zone and the indoor heat source
A_{fl}	floor area
$A_{fl,w}$	contact area between the work zone and floor
$A_{fl,s}$	contact area between the air-supply zone and floor
A_{wa}	wall area
A_{win}	window area
$A_{wa,r}$	contact area between the air-return zone and wall
$A_{wa,w}$	contact area between the work zone and wall
$A_{wa,s}$	contact area between the air-supply zone and wall
CAV	constant air volume
C_a	heat capacity of the air
C_f	heat capacity of the indoor furniture
C_{fl}	heat capacity of the floor
C_{wa}	heat capacity of the wall
DCV	demand control ventilation
DDC	direct digital control
$\|E\|$	error
ENN	Elman network neural
F	solar radiation intensity
f	density value function
$G(M)$	air amount change per unit time
G_{sa}	air mass flow of the supply air
G_{sa2}	air mass flow of the return air
$G_{sa,sw}$	air mass flow from the air-supply zone to the work zone
$G_{sa,sr}$	air mass flow from the air-supply zone to the air-return zone
$g(m)$	air amount change per unit time
$K_{fl,out}$	heat transfer coefficient between the floor outer surface and indoor air
$K_{fl,in}$	heat transfer coefficient between the floor inner surface and indoor air
K_{la}	heat transfer coefficient of the heat source
$K_{wa,out}$	heat transfer coefficient of the outer wall and outdoor air
$K_{wa,in}$	heat transfer coefficient of the inner wall and indoor air
K_{win}	heat transfer coefficient of the window and outdoor air
L	air supply volume
m	air amount
$M_{adj,i}$	humidity of the adjacent room i
M_{inr}	humidity of the air-return zone
M_{ins}	humidity of the air-supply zone
M_{inw}	humidity of the work zone
M_{sa}	humidity of the supply air
M	faces of each room
N	zones of a multi-zone building
NN	neural network
PI	proportional integral
PID	proportional integral derivative
P	pressure
$\triangle P$	Pressure difference
Q_{sunfu}	solar radiation energy absorbed by the wall outer surface
Q_{sunen}	solar radiation energy hitting the wall inner surface
Q_{inner}	energy transferred to the wall inner surface by radiation
q	amount of air infiltration
R	number of air changes
RC	resistance capacitance
RBF	radial basis function
S_c	control cycle
T	room temperature
T'	first derivative of room temperature
$T_{adj,i}$	temperature of the adjacent room i
$T_{fl,do}$	downstairs indoor temperature
$T_{fl,out}$	downstairs roof temperature
T_{fl1}	the first node temperature of the floor
T_{fl2}	the second node temperature of the floor
$T_{fl,in}$	interior surface temperature of the floor
T_{out}	outdoor temperature
T_{inr}	temperature of the air-return zone
T_{ins}	temperature of the air-supply zone
T_{inw}	temperature of the work zone
T_{la}	average temperature of the indoor heat source
T_p	predictive room temperature
T_{sa}	supply air temperature
T_{sp}	room temperature set value
T_{wa1}	temperature of the first node in the wall
T_{wa2}	temperature of the second node in the wall
$T_{wa,in}$	temperature of the wall internal surface
$T_{wa,out}$	temperature of the wall outer surface
U	disturbance vector
VAV	variable air volume
$V_{adj,i}$	volume of the adjacent room i
V_i	volume of the zone i
V_{in}	volume of the room zone
V_{inr}	volume of the air-return zone
V_{ins}	volume of the air-supply zone
V_{inw}	volume of the work zone
v	air velocity

Greek symbols

δ_{fl}	floor thickness
δ_{wa}	wall thickness
λ_{fl}	thermal conductivity of the floor
λ_{wa}	thermal conductivity of the wall
ρ_a	air density
ρ_{fl}	floor density
ρ_i	Air density of the zone i
ρ_j	Air density of the zone j
ρ_k	air density of the zone k
ρ_s	air density of the air- supply zone
ρ_w	air density of the work zone
ρ_{wa}	wall density

model can accurately calculate the energy consumption of the room and ensure indoor comfort, it does not consider the coupling of heat transfer between floors and indoor air flow in multi-zone buildings, which causes some deviation in simulating the dynamic response of room temperature. It is necessary to establish a more accurate multi-zone building mathematical model to reduce the dynamic response deviation of room temperature in the simulation process.

To realize better control of the indoor temperature of a multi-zone VAV air-conditioning system, not only an accurate multi-zone building model is required, but also an advanced algorithm to optimize the control method of the terminal temperature of the multi-zone VAV. The traditional VAV air-conditioning system uses the proportional integral (PI) algorithm to control the damper, but it cannot overcome the control system oscillations caused by sudden indoor cooling/heating loads in practical applications [8,9]. Moreover, in the indoor temperature control process, due to the heat storage of the building envelope and the instantaneous cooling/heating load variations, the room temperature response of the VAV air-conditioning system has a significant lag [10–12]. To

overcome the lag in controls, Bai et. al [15] proposed an adaptive Smith predictor to provide lag compensation to the controller, but this method requires an accurate mathematical model of the controlled object. Xu et al., [16] applied the generalized predictive control to the room temperature output of the air-conditioning system. But due to the large amount of calculation in the application process, the slow response resulted in poor control. Zhang et al., [17] applied fuzzy control to the terminal damper control of the VAV air-conditioning system. The experimental results showed that the control method could reduce the energy consumption of the system when the heating/cooling loads in each zone were the same. When there was a big difference of zone temperature, this control method had obvious shortcomings. In multi-zone buildings, the complexity of the structure and environment in each area increases the difficulty of achieving accurate control of the indoor temperature [13,14]. Therefore, there is an urgent need to apply excellent control algorithms to the terminal room temperature control of multi-zone VAV air-conditioning and improve the indoor thermal environment of multi-zone buildings.

With the rapid development of intelligent algorithms, neural networks (NN) and model prediction control algorithms have been applied to the room temperature control of VAV air-conditioning systems. Lu et al., [18] developed a prediction model by NN and genetic algorithm with nonlinear autoregressive model for indoor temperature and humidity of central air-conditioning. Kusiak et al., [19] combined the particle swarm algorithm and dynamic NN to optimize a VAV terminal, the experimental results show that the multi-objective optimization of the particle swarm algorithm could reduce the energy consumption of the air conditioning system and ensure the indoor temperature is within an acceptable range. Huang et al., [20] proposed a feed-forward NN model-based identification method to model multi-zone buildings. The model could accurately predict the change of indoor temperature after training with a large amount of data and then developed the best control strategy. Li et al., [21] applied the Elman NN to the predictive control model of the VAV air-conditioning system. Li et al., [22] presented the prediction methods for indoor temperature lag response characteristic based on time-delay NN (TDNN) and Elman NN. The results show that the Elman NN is a good prediction method for indoor temperature with small storage space and high prediction accuracy. Huang et al., [23] applied the model prediction control algorithm to the flow control device of the VAV air-conditioning system. The experimental results show that the model prediction control algorithm has good transient response (rise time, settling time and overshoot percentage) in the control. However, in the above-mentioned research, the prediction of indoor temperature is achieved through historical data and the nonlinear mapping capabilities of NNs. It is impossible to adjust the indoor temperature in real time. Although the model prediction control algorithm can control the air-conditioning terminal device, it relies too much on accurate mathematical models and is difficult to implement. In recent years, radial basis function (RBF) NN have been widely used in aerospace, medical, energy and other fields. RBF NN combined with predictive control theory has strong predictive control performance and nonlinear mapping capabilities [24–27], universal approximation and uniqueness of the best approximation property [28]. Ye et al., [29] applied the residual-corrected RBF NN to predict the air conditioning load and obtained high prediction accuracy. Sina et al., [30] used fuzzy controller and RBF NN to model and evaluate HVAC system, and the results show that RBF network has better performance than fuzzy model. Zheng et al., [31] combined proportional integral derivative (PID) control algorithm with fuzzy algorithm and RBF to establish a mathematical model of temperature control system in air conditioning room. The results show that the algorithm has short convergence time, strong anti-interference ability and superior control effect. VAV system is a typical time-delay system, which can adjust the air volume into the room according to the variation of indoor heating/cooling load. Based on the response characteristics of time-delay systems and the principle of periodic predictive control, this research proposes a mathematical model for predictive control of the room temperature by multi-zone VAV air-conditioning systems. The model is based on the multi-zone building mathematical model constructed by RC network two-node wall structure method. The developed models are validated by experimental measurements in a real building.

2. The multi-zone building mathematical model

2.1. Multi-zone building model

There are many factors that affect the change of room temperature, especially outdoor environmental factors, which makes it difficult to establish a model that can simulate the dynamic changes of the room temperature in real time. In response to this problem, this research proposes a RC network two-node wall structure method to describe and analyze the heat conduction process of the building envelope. This method can transform the complex heat transfer process of the building envelope into a simple mathematical problem and provide a new idea to establish a mathematical model of the room temperature dynamic response.

2.1.1. Room model

For the sake of analysis, a single room model is established firstly as shown in Fig. 1. The room has six sides, including an exterior wall with a window, two adjacent interior walls, an inner wall with a door, floor, and ceiling. The room is 5.9 m long, 3.9 m wide, and 3.3 m high. The room volume is about 76 m^3. The area of the window is 2 m^2. As shown in Fig. 2, the room is separated into three typical zones, including the air-supply zone, the work zone, and air-return zone. Air in each zone is assumed to be fully mixed and described by one state. Considering that the heat storage of air is smaller than that of objects such as building envelope, and the radiative heat transfer process between them is complex, so the radiative heat transfer between indoor walls and objects is ignored. To simplify the model, the energy transferred from solar radiation to the inner and outer surfaces of the wall and the energy transferred from the indoor heat source to the inner surface of the wall through radiation are set to constant values. The convective heat transfer coefficients between the walls or the heat sources and the adjacent air are considered to be constant during the simulation.

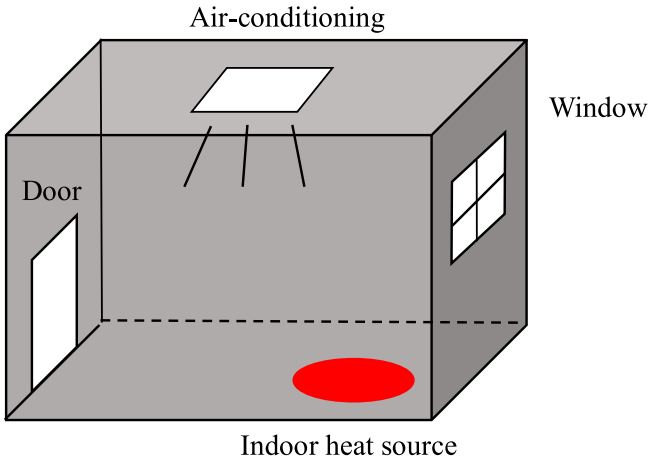

Fig. 1. A single-room model.

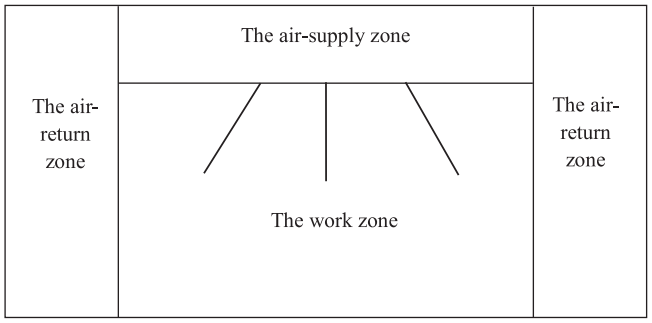

Fig. 2. Schematic for the air-conditioning room.

2.1.2. Energy and humidity balance equations of the single-room

This study uses the RC network method to describe the heat transfer through the building envelope. The RC network method can accurately describe the temperature change of the building envelope. The wall, ceiling, and floor of a room are divided into two layers as shown in Fig. 3. The heat capacity and resistance of each layer of walls, ceiling and floor are concentrated on the central node and the corresponding nodes of the indoor and outdoor contact surfaces. Among them, T_{out} is the outdoor temperature, T_{in} is the indoor temperature, T_{wa1} is the temperature of the first node of the wall, T_{wa2} is the temperature of the second node of the wall, $T_{wa,out}$ is the surface node temperature of the external wall, $T_{wa,in}$ is the internal wall surface node temperature, the box is the thermal resistance and heat capacity of the air or wall, and the symbol " C_{wa} " is the heat capacity of the wall.

The process of the room temperature change is affected by many factors. To establish a simple and universal multi-zone building mathematical model, the following assumptions must be made:

(1) The air properties are assumed to be uniform in each zone.
(2) The envelop enclosure wall is divided into two layers and the heat transfer is one-dimensional.
(3) The transmission of indoor humidity through the building envelope is not considered.

In order to analyze the heat transfer through building envelope, the wall and floor shown in Fig. 1 is divided into two layers using the RC network method. Then the energy changes of the four nodes of the wall are analyzed using the energy balance theory and the energy balance equations are established. The thickness between the outer surface of the wall and the second node of the wall is 1/4 of the thickness of the wall, and the thickness between the two nodes of the wall is 1/2 of the thickness of the wall. The thickness between the surfaces is 1/4 of the wall thickness.

For single node of room wall, the equation is shown as follows:

The energy change at a single node

$$= \textit{Incoming energy in unit time} - \textit{Outgoing energy in unit time}$$

Therefore, the energy balance equation of the outer surface of the wall, the second node of the wall, the first node of the wall and the inner surface of the wall can be obtained by Eq. (1), as follows:

$$\frac{\lambda_{wa}}{\frac{1}{4}\delta_{wa}} A_{wa}(T_{wa2} - T_{wa,out}) + A_{wa}K_{wa,out}(T_{out} - T_{wa,out}) + Q_{sunfu} = 0 \quad (2)$$

$$\frac{1}{2}\rho_{wa}\delta_{wa}A_{wa}C_{wa}\frac{dT_{wa2}}{dt} = \frac{\lambda_{wa}}{\frac{1}{2}\delta_{wa}} A_{wa}(T_{wa1} - T_{wa2}) + \frac{\lambda_{wa}}{\frac{1}{4}\delta_{wa}} A_{wa}(T_{wa,out} - T_{wa2}) \quad (3)$$

$$\frac{1}{2}\rho_{wa}\delta_{wa}A_{wa}C_{wa}\frac{dT_{wa1}}{dt} = \frac{\lambda_{wa}}{\frac{1}{4}\delta_{wa}} A_{wa}(T_{wa,in} - T_{wa1}) + \frac{\lambda_{wa}}{\frac{1}{2}\delta_{wa}} A_{wa}(T_{wa2} - T_{wa1}) \quad (4)$$

$$\frac{\lambda_{wa}}{\frac{1}{4}\delta_{wa}} A_{wa}(T_{wa1} - T_{wa,in}) + A_{wa}K_{wa,in}(T_{inr} - T_{wa,in}) + Q_{sunen} + Q_{inner} = 0 \quad (5)$$

where A_{wa} is the wall area; λ_{wa} is the thermal conductivity of the wall; $\square_{wa}$ is wall thickness; $K_{wa,out}$ is the heat transfer coefficient of the outer wall and outdoor air; $K_{wa,in}$ is the heat transfer coefficient of the inner wall and indoor air; T_{out} is the outdoor temperature; $T_{wa,out}$ is the temperature of the outer wall surface; T_{wa1} is the temperature of the first node in the wall; T_{wa2} is the temperature of the second node in the wall; $T_{wa,in}$ is the temperature of the wall internal surface; ρ_{wa} is the wall density; C_{wa} is the heat capacity of the wall; T_{inr} is the temperature of the air-return zone; Q_{sunfu} is the solar radiation energy absorbed by the external surface of the wall; Q_{sunen} is the solar radiation energy hitting the inner surface of the wall; Q_{inner} is the energy transferred to the inner surface of the wall by radiation for the indoor heat source.

Using the same method as above, the energy balance equation of the floor can be obtained:

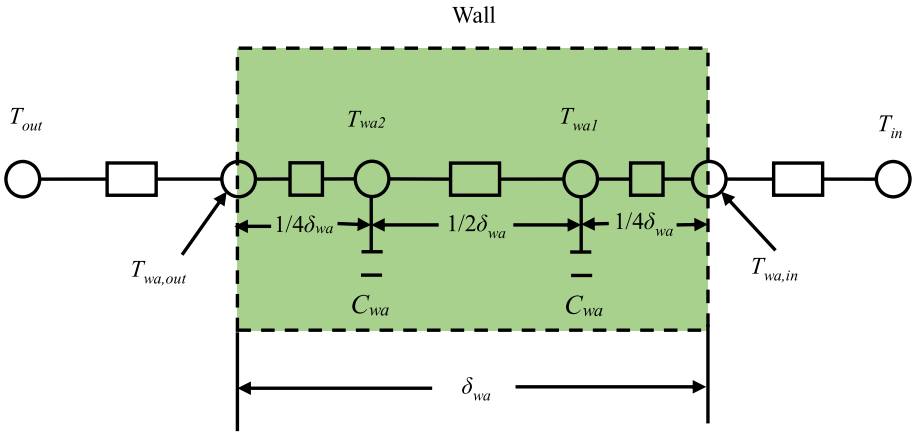

Fig. 3. Simulation method of the RC network.

$$\frac{\lambda_{fl}}{\frac{1}{4}\delta_{fl}}A_{fl}(T_{fl2}-T_{fl,out})+A_{fl}K_{fl,out}(T_{fl,do}-T_{fl,out})=0 \tag{6}$$

$$\frac{1}{2}\rho_{fl}\delta_{fl}A_{fl}C_{fl}\frac{dT_{fl2}}{dt}=\frac{\lambda_{fl}}{\frac{1}{2}\delta_{fl}}A_{fl}(T_{fl1}-T_{fl2})+\frac{\lambda_{fl}}{\frac{1}{4}\delta_{fl}}A_{fl}(T_{fl,out}-T_{fl2}) \tag{7}$$

$$\frac{1}{2}\rho_{fl}\delta_{fl}A_{fl}C_{fl}\frac{dT_{fl1}}{dt}=\frac{\lambda_{fl}}{\frac{1}{4}\delta_{fl}}A_{fl}(T_{fl,in}-T_{fl1})+\frac{\lambda_{fl}}{\frac{1}{2}\delta_{fl}}A_{fl}(T_{fl2}-T_{fl1}) \tag{8}$$

$$\frac{\lambda_{fl}}{\frac{1}{4}\delta_{fl}}A_{fl}(T_{fl1}-T_{fl,in})+A_{fl}K_{fl,in}(T_{inw}-T_{fl,in})+Q_{sunen}+Q_{inner}=0 \tag{9}$$

where λ_{fl} is the thermal conductivity of the floor; δ_{fl} is the floor thickness; $T_{fl,do}$ is the downstairs temperature; $K_{fl,out}$ is the heat transfer coefficient between the outer surface of the floor and downstairs air; $K_{fl,in}$ is the heat transfer coefficient between the inner surface of floor and indoor air; $T_{fl,out}$ is the downstairs roof temperature; T_{fl1} is the first node temperature of the floor; T_{fl2} is the second node temperature of the floor; $T_{fl,in}$ is the interior surface temperature of the floor; A_{fl} is the floor area; ρ_{fl} is the floor density; C_{fl} is the floor heat capacity; T_{ins} is the temperature of the air-supply zone. The complex process of outdoor air temperature and solar radiation transferring energy to the interior through the building envelope is reduced to simple mathematical problems, as shown in Eq.(2)-(9). The RC network two-node wall structure method is used to insert two nodes inside the building envelope, so that the established energy balance equation can reflect the energy transfer process of the building envelope more accurately.

The air-conditioning zone of the room is divided into three zones, namely the air-supply zone, the work zone, and the air-return zone, as shown in Fig. 2. To establish the energy balance equation for each zone, it is necessary to consider the energy entering and flowing out of each zone, as well as the influence of heat and air disturbance in the zone. Therefore, the energy balance equations of the air-supply zone, air- return zone and work zone can be obtained by Eq. (1), as follows:

The energy equation in the air-supply zone is:

$$\rho_a V_{ins}C_a\frac{dT_{ins}}{dt}=K_{wa,in}A_{wa,s}(T_{wa,in}-T_{ins})+K_{fl,in}A_{fl,s}(T_{fl,in}-T_{ins})+G_{sa}C_a(T_{sa}-T_{ins}) \tag{10}$$

where T_{ins} is the temperature of the air-supply zone; T_{sa} is the supply air temperature; G_{sa} is the mass flow of the supply air; V_{ins} is the volume of the air-supply zone; ρ_a is the air density; C_a is the air heat capacity; $A_{wa,s}$ is the contact area between the air-supply zone and wall; $A_{fl,s}$ is the contact area between the air-supply zone and floor.

The energy equation in the work zone is:

$$\begin{aligned}&(\rho_a V_{inw}C_a+C_f)\frac{dT_{inw}}{dt}\\&=K_{wa,in}A_{wa,w}(T_{wa,in}-T_{inw})+K_{win}A_{win}(T_{out}-T_{inw})+K_{fl,in}A_{fl,w}(T_{fl,in}-T_{inw})\\&+G_{sa}C_a(T_{sa}-T_{inw})+\sum_i\rho_a V_{adj,i}C_aR(T_{adj,i}-T_{inw})+K_{la}A_{la}(T_{la}-T_{inw})\end{aligned} \tag{11}$$

where T_{inw} is the temperature of the work zone; $A_{wa,w}$ is the contact area between the work zone and wall; K_{win} is the heat transfer coefficient of the window and outdoor air; A_{win} is the area of the window; $A_{fl,w}$ is the contact area between the work zone and wall; T_{la} is the average temperature of the indoor heat source; G_{sa} is the mass flow of the supply air; V_{in} is the volume of the work zone; C_f is the indoor furniture heat capacity; R is the number of air changes; $V_{adj,i}$ is the volume of the adjacent room i; $T_{adj,i,}$ is the temperature of the adjacent room i; K_{la} is the heat transfer coefficient of the heat source.

The energy equation in the air-return zone is:

$$\rho_a V_{inr}C_a\frac{dT_{inr}}{dt}=K_{wa,in}A_{wa,r}(T_{wa,in}-T_{inr})+G_{sa}C_a(T_{ins}-T_{inr})+G_{sa}C_a(T_{inw}-T_{inr}) \tag{12}$$

where V_{inr} is the volume of the air-return zone; $A_{wa,r}$ is the contact area between the air-return zone and wall.

The dynamic coupling model of temperature and humidity in air-conditioning rooms not only considers the influence of building envelope and indoor and outdoor environmental parameters on room temperature, but also considers the influence of indoor air humidity on room temperature. Therefore, the humidity balance equation of each zone is established to analyze the coupling relation between indoor temperature and humidity.

The humidity balance equation in the air-supply zone is:

$$V_{ins}\rho_s\frac{dM_{ins}}{dt}=G_{sa1}M_{sa}-G_{sa2}M_{inr} \tag{13}$$

where V_{ins} is the volume of the air-supply zone; ρs is the air density of the air- supply zone; M_{ins} is the air humidity of air-supply zone; G_{sa1} is the mass flow of the supply air; M_{sa} is the humidity of the supply air; G_{sa2} is the mass flow of the return air; M_{inr} is the air humidity of the air-return zone.

The humidity balance equation in the air-return zone is:

$$V_{inr}\rho_a\frac{dM_{inr}}{dt}=G_{sa,sw}M_{ins}-G_{sa,sw}M_{inw}+\sum_i\rho_a V_{adj,i}R(M_{adj,i}-M_{inw}) \tag{14}$$

where V_{inr} is the volume of the air-return zone; ρ_a is the air density of the air-return zone; $G_{sa,sw}$ is the air mass flow from the air-supply zone to the work zone; $G_{sa,sr}$ is the air mass flow from the air-supply zone to the air-return zone; M_{inw} is the air humidity of the work zone; $V_{adj,i}$ is the volume of the adjacent room i; $Madj,i$ is the humidity of the adjacent room i.

The humidity equation in the work zone is:

$$\rho_w V_{inw}\frac{dM_{inw}}{dt}=G_{sa}M_{ins}-G_{sa}M_{inw}+\sum_i\rho_w V_{adj,i}C_aR(M_{adj,i}-M_{inw}) \tag{15}$$

where $Vinw$ is the volume of the work zone; ρw is the air density of the work zone; $Minw$ is the humidity of the work zone.

2.1.3. Solution of the dynamic temperature and humidity

Energy balance equations Eq.(2) - (12) of the wall, floor joints and air-conditioning room are combined, variables $T_{wa,out}$, $T_{wa,in}$, $T_{fl,out}$ and $T_{fl,in}$ are eliminated, and the temperature response equation of each node of the wall and each zone in a single room can be obtained:

$$\begin{aligned}\frac{1}{2}\rho_{wa}\delta_{wa}A_{wa}C_{wa}\frac{dT_{wa1}}{dt}&=\left(\frac{4\frac{\lambda_{wa}}{\delta_{wa}}A_{wa}}{1+\frac{\delta_{wa}K_{wa,in}}{4\lambda_{wa}}}-6\frac{\lambda_{wa}}{\delta_{wa}}A_{wa}\right)T_{wa1}+2\frac{\lambda_{wa}}{\delta_{wa}}A_{wa}T_{wa2}\\&+\frac{K_{wa,in}A_{wa}}{1+\frac{\delta_{wa}K_{wa,in}}{4\lambda_{wa}}}T_{inr}+\frac{Q_{sunen}+Q_{inner}}{1+\frac{\delta_{wa}K_{wa,in}}{4\lambda_{wa}}}\end{aligned} \tag{16}$$

$$\begin{aligned}\frac{1}{2}\rho_{wa}\delta_{wa}A_{wa}C_{wa}\frac{dT_{wa2}}{dt}&=2\frac{\lambda_{wa}}{\delta_{wa}}A_{wa}T_{wa1}+\left(\frac{4\frac{\lambda_{wa}}{\delta_{wa}}A_{wa}}{1+\frac{\delta_{wa}K_{wa,out}}{4\lambda_{wa}}}-6\frac{\lambda_{wa}}{\delta_{wa}}A_{wa}\right)T_{wa2}\\&+\frac{K_{wa,out}A_{wa}}{1+\frac{\delta_{wa}K_{wa,out}}{4\lambda_{wa}}}T_{out}+\frac{Q_{sunfu}}{1+\frac{\delta_{wa}K_{wa,out}}{4\lambda_{wa}}}\end{aligned} \tag{17}$$

$$\begin{aligned}\frac{1}{2}\rho_{fl}\delta_{fl}A_{fl}C_{fl}\frac{dT_{fl1}}{dt}&=\left(\frac{4\frac{\lambda_{fl}}{\delta_{fl}}A_{fl}}{1+\frac{\delta_{fl}K_{fl,in}}{4\lambda_{fl}}}-6\frac{\lambda_{fl}}{\delta_{fl}}A_{fl}\right)T_{fl1}+2\frac{\lambda_{fl}}{\delta_{fl}}A_{fl}T_{fl2}\\&+\frac{K_{fl,in}A_{fl}}{1+\frac{\delta_{fl}K_{fl,in}}{4\lambda_{fl}}}T_{ins}+\frac{Q_{sunen}+Q_{inner}}{1+\frac{\delta_{fl}K_{fl,in}}{4\lambda_{fl}}}\end{aligned} \tag{18}$$

$$\frac{1}{2}\rho_{fl}\delta_{fl}A_{fl}C_{fl}\frac{dT_{fl2}}{dt}=\left(\frac{4\frac{\lambda_{fl}}{\delta_{fl}}A_{fl}}{1+\frac{\delta_{fl}K_{fl,out}}{4\lambda_{fl}}}-6\frac{\lambda_{fl}}{\delta_{fl}}A_{fl}\right)T_{fl2}+2\frac{\lambda_{fl}}{\delta_{fl}}A_{fl}T_{fl1}+\frac{A_{fl}K_{fl,out}}{1+\frac{\delta_{fl}K_{fl,out}}{4\lambda_{fl}}}T_{out} \tag{19}$$

$$\begin{aligned}(\rho_a V_{inw}C_a+C_f)\frac{dT_{inw}}{dt}&=K_{wa,in}A_{wa,w}\left(\frac{4\frac{\lambda_{wa}}{\delta_{wa}}T_{wa1}+K_{wa,in}T_{inr}}{4\frac{\lambda_{wa}}{\delta_{wa}}+K_{wa,in}}-T_{inw}\right)+K_{win}A_{win}(T_{out}-T_{inw})\\&+K_{fl,in}A_{fl,w}\left(\frac{4\frac{\lambda_{fl}}{\delta_{fl}}T_{fl1}+K_{fl,in}T_{ins}}{4\frac{\lambda_{fl}}{\delta_{fl}}+K_{fl,in}}-T_{inw}\right)+G_{sa}C_a(T_{sa}-T_{inw})\\&+\textstyle\sum_i\rho_a V_{adj,i}C_aR(T_{adj,i}-T_{inw})+K_{la}A_{la}(T_{la}-T_{inw})\end{aligned} \tag{20}$$

$$\begin{aligned}\rho_a V_{ins}C_a\frac{dT_{ins}}{dt}&=K_{wa,in}A_{wa,s}\left(\frac{4\frac{\lambda_{wa}}{\delta_{wa}}T_{wa1}+K_{wa,in}T_{inr}}{4\frac{\lambda_{wa}}{\delta_{wa}}+K_{wa,in}}-T_{ins}\right)\\&+K_{fl,in}A_{fl,s}\left(\frac{4\frac{\lambda_{fl}}{\delta_{fl}}T_{fl1}+K_{fl,in}T_{ins}}{4\frac{\lambda_{fl}}{\delta_{fl}}+K_{fl,in}}-T_{ins}\right)+G_{sa}C_a(T_{sa}-T_{ins})\end{aligned} \tag{21}$$

$$\begin{aligned}\rho_a V_{inr}C_a\frac{dT_{inr}}{dt}&=K_{wa,in}A_{wa,r}\left(\frac{4\frac{\lambda_{wa}}{\delta_{wa}}T_{wa1}+K_{wa,in}T_{inr}}{4\frac{\lambda_{wa}}{\delta_{wa}}+K_{wa,in}}-T_{inr}\right)\\&+G_{sa}C_a(T_{ins}-T_{inr})+G_{sa}C_a(T_{inw}-T_{inr})\end{aligned} \tag{22}$$

By Eq.(16) - (22), the change of indoor temperature in a multi-zone room is not only related to the instantaneous cooling load caused by outdoor air temperature, solar radiation and heat transfer into the room by indoor heat sources, but also related to the indoor temperature, supply air volume, return air volume, supply air temperature and other variables of the VAV air-conditioning system, as well as the room temperature of the adjacent room.

Eq.(13)-(22) is written in the matrix form of first-order differential equation as follows:

$$C\frac{dX}{dt}=AX+BU \tag{23}$$

where A, B, C are correlation coefficients.

The system variable vector is:

$$X=[T_{wa1},T_{wa2},T_{fl1},T_{fl2},T_{ins},T_{inw},T_{inr},M_{inw}]^T \tag{24}$$

The disturbance vector is:

$$U=[T_{out},G_{sa},T_{la},T_{adj,i},M_{adj,i},\frac{Q_{sunen}+Q_{inner}}{1+\frac{\delta_{wa}K_{wa,in}}{4\lambda_{wa}}},\frac{Q_{sunfu}}{1+\frac{\delta_{wa}K_{wa,out}}{4\lambda_{wa}}},\frac{Q_{sunen}+Q_{inner}}{1+\frac{\delta_{fl}K_{fl,in}}{4\lambda_{fl}}}] \tag{25}$$

Multiplying both sides of the equation with C^-, we have:

$$\frac{dX}{dt}=C^-AX+C^-BU \tag{26}$$

Eq.(26) is the dynamic response equation of indoor temperature and humidity change in a single air-conditioning room. Because the temperature and humidity in the air-conditioning room will change dynamically with time due to indoor and outdoor environmental factors. Therefore, Eq.(26) is integrated over time, and the solution of X is:

$$X(t)=e^{C^-AX}X(0)+e^{C^-AX}\int_0^t e^{-eC^-A\tau}C^-BU(\tau)d\tau \tag{27}$$

2.1.4. Multi-zone room air coupling model

The air in a multi-zone room generally flows through two channels, windows and doors. During the air flow, the energy and quality of the indoor air are exchanged with the surrounding air. According to the law of conservation of mass, the amount of air flowing into and out of a room is conserved.

In this study, the multi-zone building is divided into N zones. Because of different room structures in the building, assuming each room is composed of M faces, and there are multiple common faces in each room of the whole building. When there is pressure difference between the two zones, hot-pressing ventilation will occur in these two zones. The Bernoulli principle can be used to calculate the air flow exchanged between any two zones i and j in the multi-zone building. If the air in zone i is stationary relative to zone j, then:

$$q^{i-j}=v_j\cdot A=\sqrt{\frac{2P_i}{\rho_i}-\frac{2P_j}{\rho_j}}\cdot A \tag{28}$$

where P_i is the pressure of the zone i; P_j is the pressure of the zone j; ρ_i is the air density of the zone i; ρ_j is the air density of the zone j; v_j is the air velocity of the zone j penetrating into the zone i through doors and windows; A is the area between the zone i *and* zone j that can be permeated by air.

Take any zone i in the multi-zone building according to the law of conservation of mass, then:

$$\begin{aligned}g(m_i)=\frac{\partial m_i}{\partial t}&=\rho_i\frac{\partial V_i}{\partial t}+V_i\frac{\partial\rho_i}{\partial t}=\sum_{k=1}^{n}f(\rho_k,\rho_i).q^{i-k}\\f(\rho_k,\rho_i)&=\begin{cases}\rho_k,\Delta P>0\\\rho_i,\Delta P<0\end{cases}\end{aligned} \tag{29}$$

where m_i is the air amount in the zone i; $g(m_i)$ is the change of air amount in the zone i per unit time; ρ_i is the air density in the zone i; ρ_k is the air density in the zone k adjacent to the zone i; V_i is the volume of the zone i; q^{i-k} is the amount of air infiltration through windows and doors between the zone i and zone j; $f(\rho_k,\rho_i)$ is the density value function of the zone i and zone k; ΔP is the pressure difference between the zone k and zone i ($\Delta P=P_k-P_i$).

According to the law of conservation of mass, the amount of air flowing into and out in a zone is also conserved, then:

$$g(m_i)=0 \tag{30}$$

The whole building is divided into N zones, and the change of air amount per unit time in a zone is as follows:

$$g_i(m_1,m_2,...m_{i-1},...,m_{i+1},...,m_N)=\sum_{k=1}^{n}f(\rho_k,\rho_i).q^{i-k},i=1,2,...,N. \tag{31}$$

where $g_i(m_1,m_2,...m_{i-1},...,m_{i+1},...,m_N)$ is the variation of air amount per unit time in zone i under the combined action of N-1 zones.

For the multi-zone building, each zone also satisfies the law of mass conservation, then:

$$g_i(m_1,m_2,...m_{i-1},...,m_{i+1},...,m_N)=0 \tag{32}$$

The variation of air amount in unit time of N zones in the whole building can be expressed as a vector form:

$$G(M)=\begin{Bmatrix}g_1(y)\\g_2(y)\\\cdot\\\cdot\\\cdot\\g_N(y)\end{Bmatrix},M=\begin{Bmatrix}m_1\\m_2\\\cdot\\\cdot\\\cdot\\m_N\end{Bmatrix},y=\begin{Bmatrix}m_1\\m_2\\\vdots\\m_{i-1}\\\vdots\\m_{i+1}\\\vdots\\m_N\end{Bmatrix},0=\begin{Bmatrix}0\\0\\\cdot\\\cdot\\\cdot\\0\end{Bmatrix},i=1,2,...,N. \tag{33}$$

where $G(M)$ is the change of air amount per unit time in the whole building. For the multi-zone building, the whole building also satisfies the law of mass conservation, then:

$$G(M) = 0 \tag{34}$$

2.1.5. Establishment of multi-zone building model

In a multi-zone building, when analyzing the factors that cause the temperature and humidity changes in a room, the indoor environment parameters of the adjacent room can be used as the outdoor environment parameters of the room to establish the energy balance equations of each node. Extend the single-zone mathematical model to the multi-zone mathematical model, establish the coupling model of temperature and humidity in multi-zone building, and solve the dynamic response equation of the temperature in each room, so as to obtain the temperature and humidity of each room in the whole building. The single-room model is $C\frac{dX}{dt} = AX + BU$. Assuming a building has n rooms numbered from 1 to n, then the multi-zone model shall be:

$$\begin{bmatrix} C_1 & 0 & 0 & 0 & 0 \\ 0 & C_2 & 0 & 0 & 0 \\ 0 & 0 & C_3 & 0 & 0 \\ \vdots & \vdots & \vdots & \vdots & \vdots \\ 0 & 0 & 0 & 0 & C_n \end{bmatrix} \begin{bmatrix} \frac{dX_1}{dt} \\ \frac{dX_2}{dt} \\ \frac{dX_3}{dt} \\ \vdots \\ \frac{dX_n}{dt} \end{bmatrix} = \begin{bmatrix} A_1 & 0 & 0 & 0 & 0 \\ 0 & A_2 & 0 & 0 & 0 \\ 0 & 0 & A_3 & 0 & 0 \\ \vdots & \vdots & \vdots & \vdots & \vdots \\ 0 & 0 & 0 & 0 & A_n \end{bmatrix} \begin{bmatrix} X_1 \\ X_2 \\ X_3 \\ \vdots \\ X_n \end{bmatrix} + \begin{bmatrix} B_1 & 0 & 0 & 0 & 0 \\ 0 & B_2 & 0 & 0 & 0 \\ 0 & 0 & B_3 & 0 & 0 \\ \vdots & \vdots & \vdots & \vdots & \vdots \\ 0 & 0 & 0 & 0 & B_n \end{bmatrix} \begin{bmatrix} U_1 \\ U_2 \\ U_3 \\ \vdots \\ U_n \end{bmatrix} \tag{35}$$

The solution to Eq. (35) is the same to Eq. (26), then X_n as:

$$X_n(t) = e^{C_n^- A_n X_n} X_n(0) + e^{C_n^- A_n X_n} \int_0^t e^{-eC_n^- A_n \tau} C_n^- B_n U_n(\tau) d\tau \tag{36}$$

2.2. Predictive control model of room temperature

The multi-zone building mathematical model constructed by the energy balance theory can only dynamically adjust the room temperature according to the change of air supply, the set value of air supply temperature and the change of instantaneous cooling load entering the room through various channels. However, the theoretical model cannot dynamically adjust the room temperature by adjusting the opening degree of VAV BOX air damper and the speed of the supply fan. This leads to the lag phenomenon of room temperature on the opening degree of VAV BOX air damper, fan speed and other adjustment changes. In order to solve the above problems, this study uses RBF NN. The structure of RBF NN is composed of input layer, hidden layer and output layer. It can approximate any nonlinear function, and it has the ability of online learning and prediction. According to the room real-time situation, it can control the opening degree of the VAV BOX air damper and the speed of the fan, so as to control the controlled amount of the air supply and make the room temperature reach the target value.

Based on the periodic predictive control principle of time-delay systems, the predictive control model of a room temperature is established by using the RBF NN and multi-zone building mathematical model. In the predictive control model, the room temperature can be obtained by inputting the opening degree of the air damper and the fan speed. The multi-zone building mathematical model and RBF NN model constitute the parallel structure shown in Fig. 4. The supply air volume $L(\tau-1)$, disturbance $U(\tau-1)$, room temperature $T(\tau-1)$ simulated by the multi-zone building mathematical model and room temperature first derivative $T'(\tau-1) = T(\tau-1) - T(\tau-2)$ are used as the input of the RBF NN model to predict the room temperature $T_p(\tau)$ at the next moment. The deviation E between the output of the multi-zone building model and RBF NN model is calculated in the training process of RBF NN. In order to ensure the prediction accuracy of RBF NN, it is necessary to set a threshold for E, thus forming a supervised learning structure. The threshold was set as 0.6 according to the results of multiple training of RBF NN. Under the condition of $|E| \leq 0.6$, the trained RBF NN model can well describe the dynamic characteristics of the room temperature delay system. The room temperature $T_p(\tau)$ predicted by the RBF NN model is fed back to the input end of the RBF NN and the PI algorithm. The RBF NN model predicts the room temperature $T_p(\tau+1)$ at the next moment according to room temperature $T_p(\tau)$. The PI algorithm calculates the opening degree of the terminal air damper according to the deviation between the room temperature predicted value $T_p(\tau)$ and the room temperature set value T_{sp}. The terminal air damper periodically adjusts the opening degree according to the control cycle S_c, and adjusts the air supply volume L into the room, which causes the change of static pressure of the pipeline. The direct digital control (DDC) of the fan inverter adjusts the speed of the fan in real time according to the static pressure change measured by the static pressure sensor in the pipeline, and then adjusts the total air supply to maintain the static pressure of the air supply pipeline system. By controlling the opening degree of the air damper and the speed of the fan, the air volume into the room is adjusted, and the room temperature is adjusted. If $|E| > 0.6$, the RBF NN is retrained by using the room temperature calculated by the multi-zone building model.

This paper applies the predictive control model to the terminal control device of a VAV air-conditioning system and adopts the VAV air-conditioning pressure-dependent terminal control that can effectively suppress the influence of the terminal inlet pressure disturbance on the room temperature.

The specific implementation process of the predictive control model is as follows:

(1) The system collects parameters that affect the room temperature, including the position of the VAV terminal air damper, fan speed, air supply temperature and air supply volume.
(2) Calculate the predicted room temperature by the RBF NN.
(3) According to the deviation between the predicted value of the room temperature and the set value, calculate the opening degree of the terminal air damper and output the air damper position according to the control cycle.

3. Validation of Multi-zone building model

In order to verify the multi-zone building model established in this study can real time simulate the dynamic change of room temperature, the temperature and humidity of a single room are simulated and analyzed firstly. Then the room temperature of each room in the multi-zone building is simulated and analyzed based on results of the single-room analysis. The calibration of experimental instruments for measuring building envelope parameters was made before the experiment. The building envelope and indoor and outdoor environmental parameters as shown in Table 1.

3.1. Single-room simulation

In order to improve the accuracy of the model, the mathematical model of a single room is first verified. A single room shown in Fig. 1, the initial temperature of the room is set at 15 °C, and the initial room humidity ratio is set at 11.5 g/(kg dry air). Under the condition of cold air transported to a single room, the dynamics of the room temperature and humidity of a single room, the temperature of each node of the wall and the floor were simulated in the MATLAB software according to the building envelope and indoor and outdoor environmental parameters.

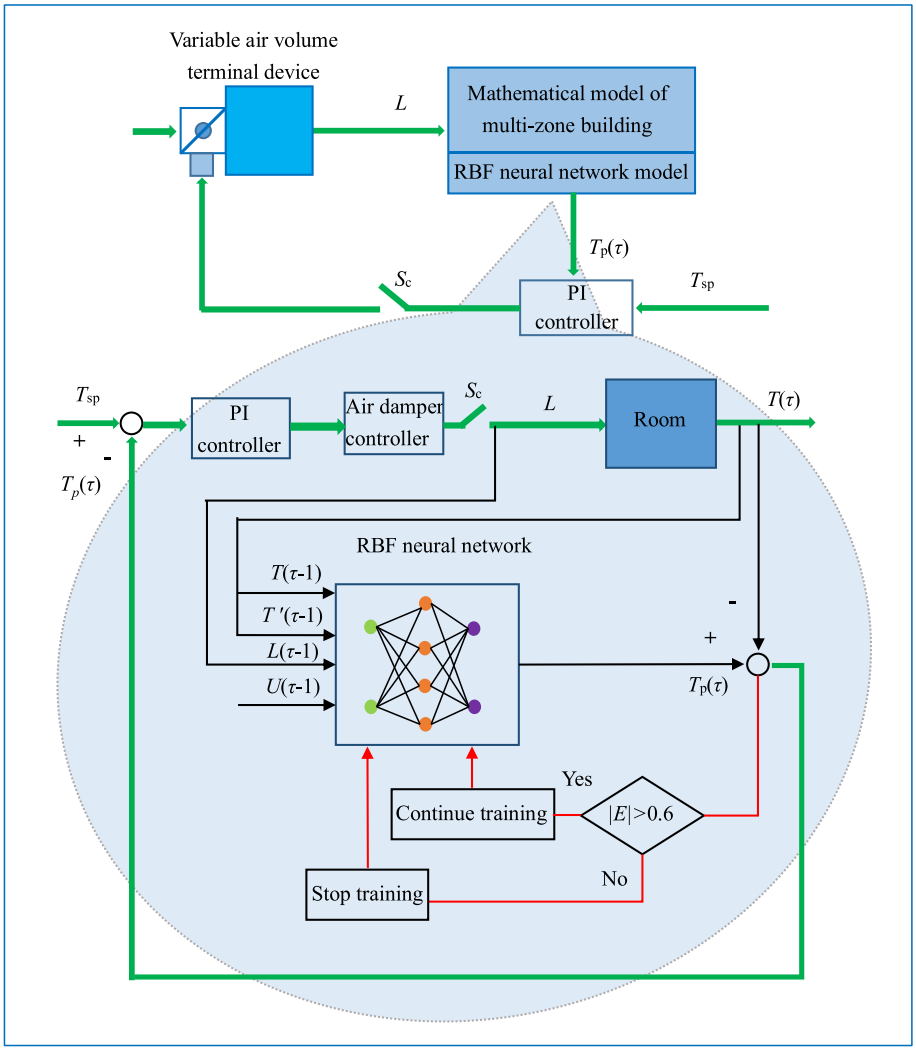

Fig. 4. RBF NN-based periodic predictive control model of room temperature time-delay system.

Table 1
The building envelope and indoor and outdoor environmental parameters.

Variables	Parameters	Variables	Parameters
ρ_{wa}	2800 kg/m^3	K_{win}	3 W/(m^2·℃)
δ_{wa}	0.2 m	A_{win}	2 m^2
A_{wa}	12.87 m^2	C_f	10000 J/(kg·℃)
C_{wa}	1000 J/(kg·℃)	$T_{wa,out}$	19.5 ℃
λ_{wa}	1.6 W/(m·℃)	$K_{wa,out}$	12 W/(m^2·℃)
$K_{wa,in}$	5 W/(m^2·℃)	$K_{fl,out}$	6 W/(m^2·℃)
V	76 m^3	ρ_{fl}	2500 kg/m^3
C_a	1000 J/(kg·℃)	δ_{fl}	0.2 m
T_{sa}	10 ℃	C_{fl}	950 J/(kg·℃)
λ_{fl}	12.8 W/(m·℃)	$T_{fl,out}$	18.5 ℃
T_{in}	15 ℃	F	3386.11 W/m^2
$K_{fl,in}$	5 W/(m^2·℃)	M_{sa}	10.6 g/(kg dry air)
A_{fl}	23.01 m^2	M_{in}	11.5 g/(kg dry air)
T_{out}	23 ℃	Q_{sunfu}	0.4 KJ
ρ_a	1.34 kg/m^3	Q_{suner}	0.5 KJ
G_{sa}	0.05 kg/s	Q_{inner}	0.35 KJ

The simulation results are shown in Fig. 5. Fig. 5(a) shows the dynamic response curves of the temperature of each node of the wall and floor and room temperature simulated by MATLAB software, and Fig. 5(b) shows the dynamic response curve of room humidity ratio simulated by MATLAB software. As shown in Fig. 5(a), the temperature at each point changes slowly after 1000 s, and the temperature of the first node of the wall and floor is basically stable after 1000 s. While the temperature of the second node of the wall and floor still changes slightly after 1000 s, especially the second node of the wall. The room temperature still changes slightly after 1000 s, tends to be stable around 2000 s, and keeps at 12.4℃. From the simulation data of the single room, the temperature of each node of the wall and floor is significantly higher than the room temperature, and the stabilized room temperature is also higher than the supply air temperature. It shows that the outdoor environment transfers energy to the interior through the building envelope and participates in the change of room temperature; it also verifies that the single-room model can simulate the dynamic change of the room temperature. It also shows that the RC network two-node wall structure method to solve the energy changes of the building walls and floors is correct, and provides a theoretical method to establish a multi-zone building model. As shown in Fig. 5(b), although the room air humidity ratio is constantly changing, the variation is small, and the room air humidity ratio is between 10.6 g/(kg dry air) and 11.5 g/(kg dry air). The humidity ratio tends to be stable and close to M_{sa}.

3.2. Multi-room simulation

Fig. 6 is a three-story office building with six rooms each floor and a basement. The building is located in Dalian, China, which belongs to a cold region. The building is separated by a corridor.

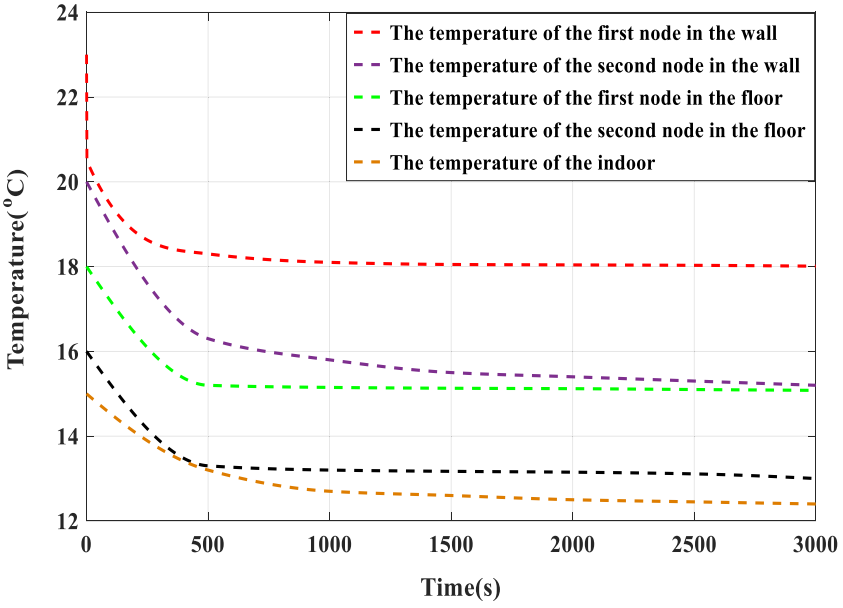

(a)

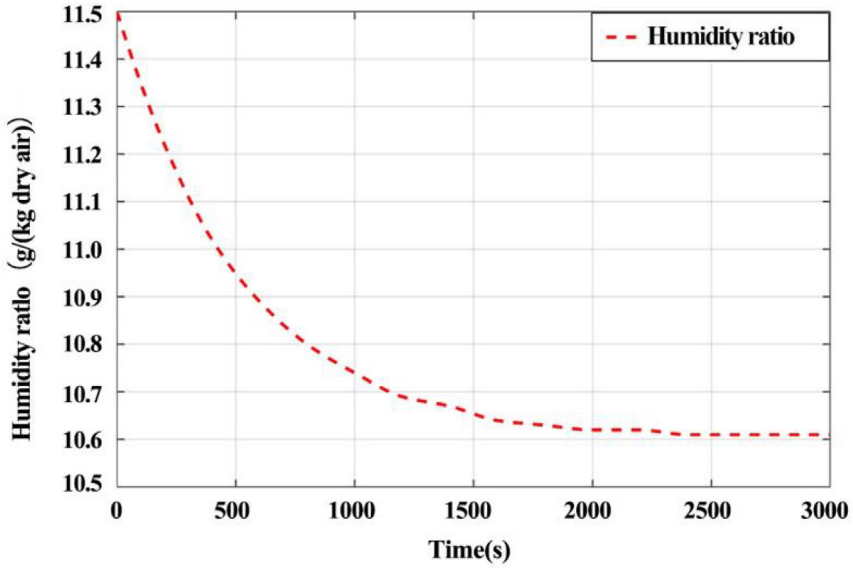

(b)

Fig. 5. Response curves of temperature and humidity ratio for the single-room: (a) Temperature curves of different nodes and indoor environments, (b) The predicted curve of indoor humidity ratio.

This study only simulated the front section because this building is symmetric. Each room in the building has the same structure as the room in the single-room model, and the building envelope has the same parameters. In order to verify the accuracy of multi-zone building model, this research carries out experimental verification in the above-mentioned building for the indoor temperature changes without/with air conditioning. The scenario without air conditioning is to simulate the accidental shut down of the air conditioning system. The simulation result of the single room shows that the indoor humidity ratio has a small change, so this section does not consider the humidity transport.

3.2.1. Simulation without air conditioning

The experiment was carried out in January. Initially, the same heat was provided in each room, and the room temperature in each room reached a steady state after a period of time. Then the heating in all rooms was turned off, and the temperature in the room was measured with an automatic temperature recorder. The automatic temperature recorder was installed in the middle of the room and 1.5 m from the ground, and recorded the room temperature every minute. This measurement lasted for 2000 s. During the experiment, the experimental room had no changes in heating load such as heat dissipation from electrical equipment and human body, so the room heating load did not change much and could be regarded as unchanged. The measured average temperature of the basement was 3℃ in the process of collecting room temperature, and the average outdoor air temperature and the average solar radiation intensity were −6℃ and 3386.11 W/m^2. The initial temperature of each room in the experiment is different due to different locations and different operation conditions.

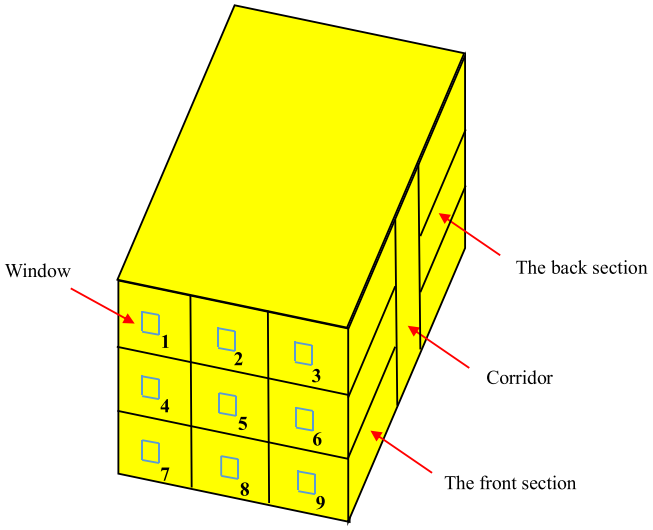

Fig. 6. The building structures.

The multi-zone building model is used to simulate the dynamic change of room temperature when the air-conditioning system stops suddenly. The simulation results are shown in Fig. 7. The real-time change curves of the measured temperature values and the simulated temperature values of each room are almost the same. As shown in Fig. 7(a), during the period of 500 s-1000 s in Room 1, the simulated temperature value is larger than the measured temperature value, but the difference between them is less than 0.5 °C. As shown in Fig. 7(b), the measured temperature is greater than the simulated temperature during the period of 1000 s-2000 s in Room 7, but the difference between them is less than 0.5 °C. The real-time changing simulated temperature value of other rooms is almost the same as the measured temperature value, and the difference between them is less than 0.2 °C. The large difference between the measured and simulated temperature values of Room 1 and Room 7 may be caused by some factors such as the time delay of the measuring instrument. In general, the multi-zone building model can accurately simulate the dynamic change of room temperature when the air-conditioning system suddenly stops in real time. Room 1 is on the top floor, and the room temperature drops very quickly, falling below 0 °C after 1400 s as shown in Fig. 7(a). Because Room 2 is in the middle of the top floor, the temperature drops to 3 °C after 1400 s as shown in Fig. 7(b). As shown in Fig. 7(d), the temperature in Room 4 is higher than that in Room 1, because it is a middle floor and has less heat loss. The temperature of Room 5 is higher than that of other rooms, and the room temperature remains 7℃ after 2000 s as shown in Fig. 7(e). This is because the room is located in the middle of the whole building

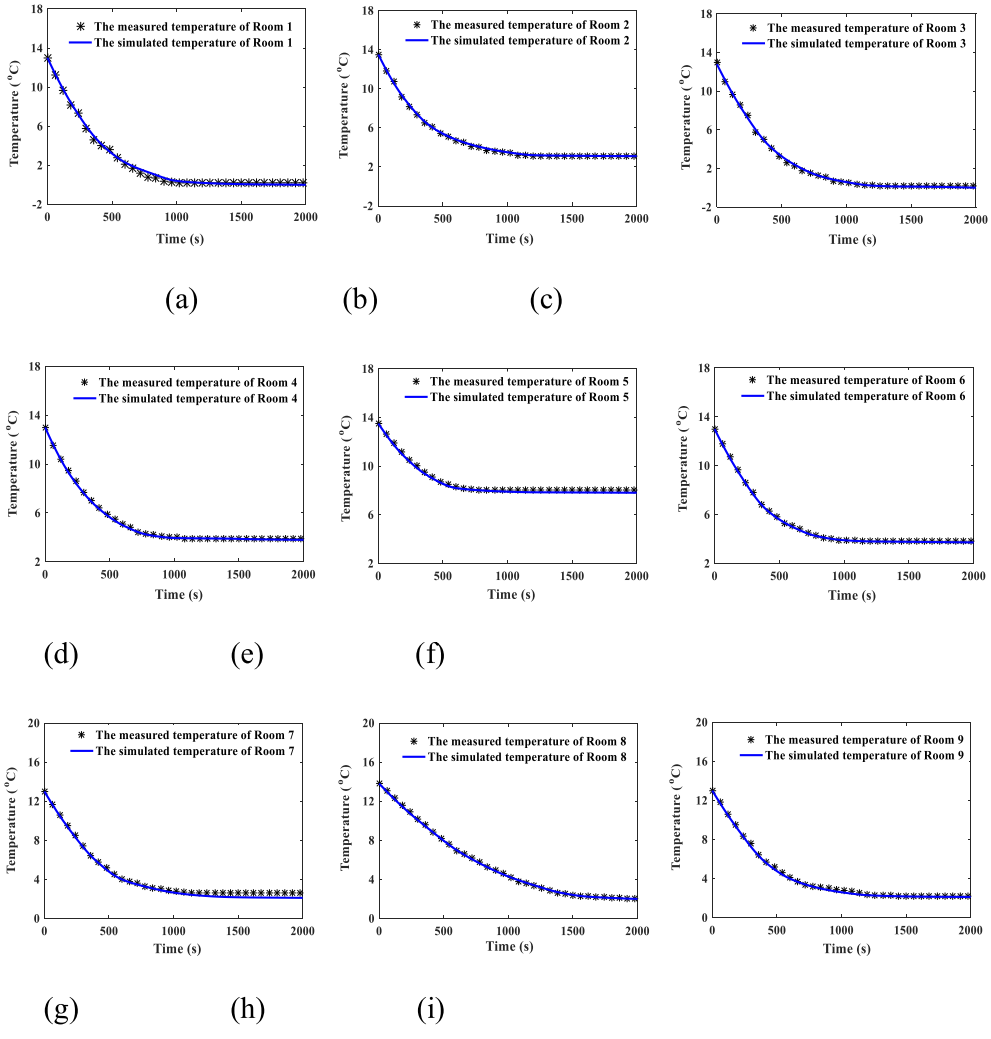

Fig. 7. Temperature response curves of rooms without air conditioning: (a) Temperature response curves of Room 1, (b) Temperature response curves of Room 2, (c) Temperature response curves of Room 3, (d) Temperature response curves of Room 4, (e) Temperature response curves of Room 5, (f) Temperature response curves of Room 6, (g) Temperature response curves of Room 7, (h) Temperature response curves of Room 8, (i) Temperature response curves of Room 9.

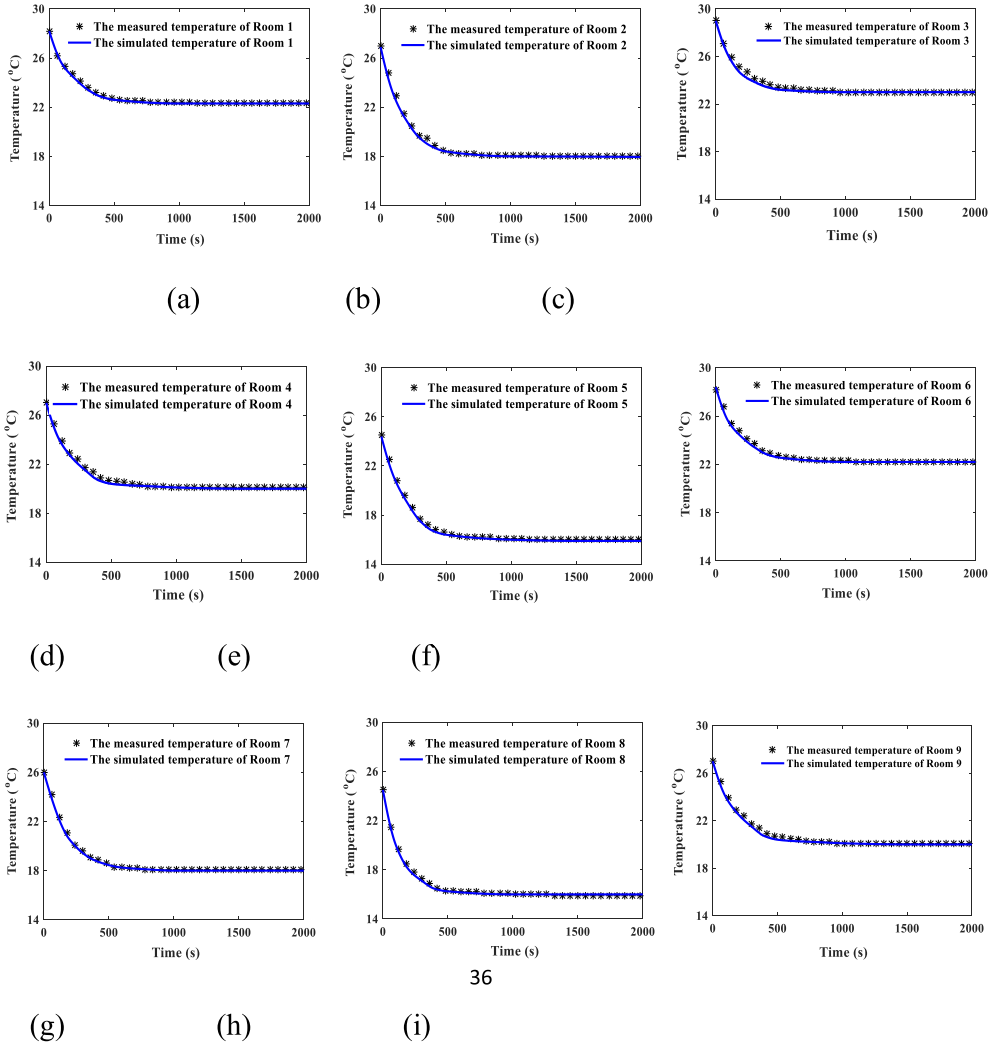

Fig. 8. Temperature response curves of rooms with air-conditioning: (a) Temperature response curves of Room 1, (b) Temperature response curves of Room 2, (c) Temperature response curves of Room 3, (d) Temperature response curves of Room 4, (e) Temperature response curves of Room 5, (f) Temperature response curves of Room 6, (g) Temperature response curves of Room 7, (h) Temperature response curves of Room 8, (i) Temperature response curves of Room 9.

and has minimal heat loss. As shown in Fig. 7(g)-(i), When the room temperature is stable, the temperature in Rooms 7, 8, and 9 are around 2 °C. Since these rooms are located on the first floor and the basement temperature is higher than the outdoor temperature, the heat loss of these rooms is small. It can be found that considering indoor air convection and heat transfer between the upper and lower floors, the multi-zone building model can simulate the dynamic changes of room temperature more accurately.

3.2.2. Simulation with air conditioning

Based on the above-mentioned experimental platform and same setup, the experiment was carried out in July under the condition that the building was air-conditioned. The initial condition is to turn off the air-conditioning in the room so that the temperature reached a stable state. Turning on the air-conditioning indicates the beginning of the experiment, and the automatic temperature recorder is used to measure the room temperature at the same time. The supply air temperature is 10 °C and the mass flow rate of each room is 0.08 kg/s. The air damper opening degree of each room is the same. During the measurement, the average temperature in the basement was 24℃. The average outdoor temperature was 31℃, and the average solar radiation intensity was 813.89 W/m^2. Similarly, the measurement also lasted for 2000 s.

The multi-zone building model established in this study is used to simulate the dynamic change of room temperature when the air-conditioning system is in normal operation. The simulation results are shown in Fig. 8. The measured temperature and the simulated temperature of each room are synchronized and drop rapidly with time, and the real-time difference between them is less than 0.2 °C. It shows that the multi-zone building model can accurately simulate the dynamic changes of room temperature with air-conditioning in real time. The temperature of each room reaches a stable state after 1000 s, but the temperature of each room is different, which shows that the multi-zone building model can accurately and real-time simulate the dynamic change of the room temperature with the air-conditioning in different external environments.

For multi-room, the location and usage of each room are different. When the indoor air temperature of the adjacent room of a certain room is higher, the temperature of the room will drop more slowly. However, due to the small heat capacity of the indoor air in adjacent rooms, the heat transfer through the wall is not large, and the temperature change of the room has little effect, and the outdoor air temperature is the main factor that affects the room temperature change.

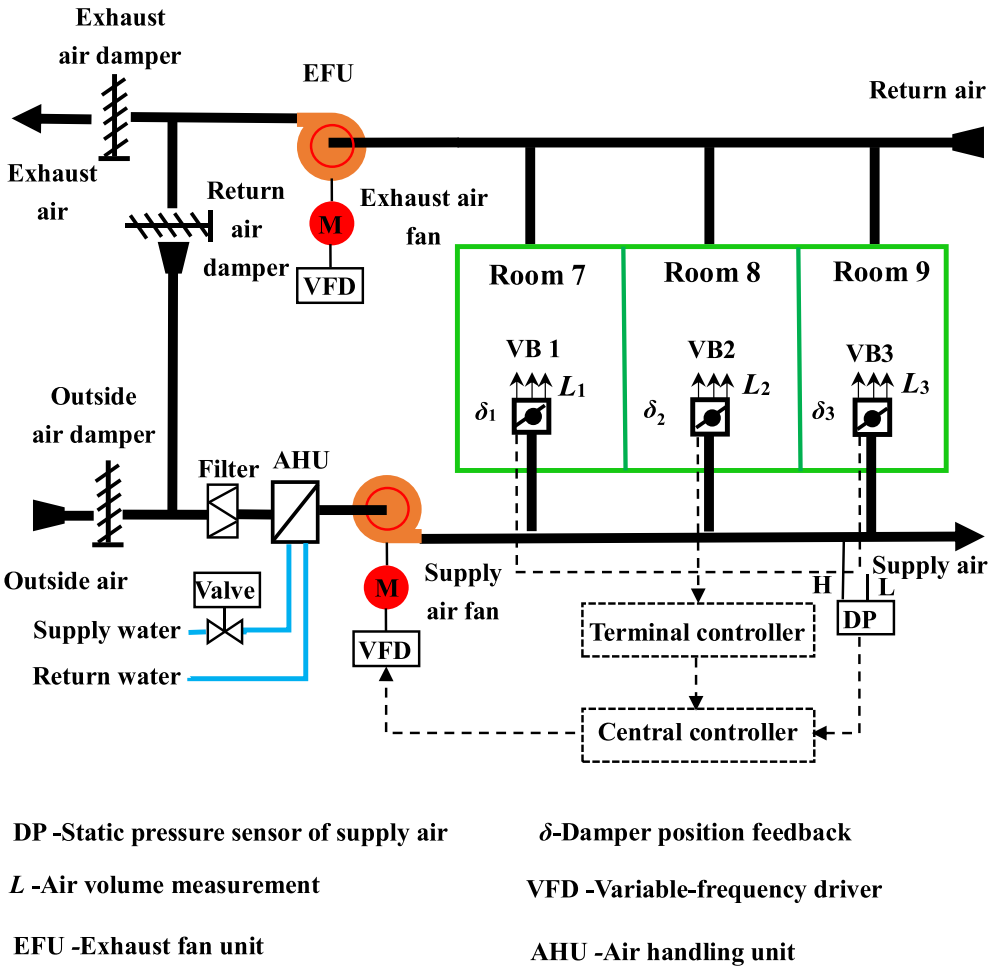

Fig. 9. Schematic diagram of a single duct multi-zone VAV air-conditioning system.

Table 2
Main electromechanical equipment of VAV system.

Name	Equipment	Parameter
AHU	Air Handling unit	Air volume: 1500 m^3/h, Refrigerating capacity: 10 kW
EFU	Exhaust fan unit	Air volume: 1300 m^3/h, Motor power: 5 kW
VB 1	VAV Box 1	Air volume: 0–315 m^3/h
VB 2	VAV Box 2	Air volume: 0–315 m^3/h
VB 3	VAV Box 3	Air volume: 0–315 m^3/h

4. Predictive control of multi-zone VAV air-conditioning system

According to theory of time-delay system theory for VAV air-conditioning room temperature, the room temperature delay time to the terminal air damper adjusting is determined first by the experimental study of the room temperature delay response characteristics. The periodic predictive control model of room temperature time-delay system based on RBF NN and multi-zone building model is applied to the terminal control experimental platform in multi-zone VAV air-conditioning system to verify its control effect. At the same time, the indoor real-time temperature of the terminal control experimental platform, the air volume into the room and terminal air damper position are measured when the predictive control model is running. In order to illustrate the advantages of predictive control model in multi-zone VAV air-conditioning system. The predictive control model in this study is compared with Elman NN predictive control model for the control effect of multi-zone VAV air-conditioning system under the same conditions.

4.1. Room temperature delay response characteristics

With the variation of the terminal air damper opening degree, the air supply volume of VAV terminal box changes, which further affects the indoor air temperature. The dynamic response of room temperature is delayed during the air supply volume adjustment process. In order to study the room temperature delay time to the terminal air damper adjusting, this study uses an experimental platform for a multi-zone VAV air-conditioning system, which is located in Rooms 7, 8 and 9 shown in Fig. 6. The structure of the multi-zone VAV air-conditioning systems shown in Fig. 9, each room has a VAV box. The supply air static pressure sensor is located on the main supply air pipe. The main equipment parameters of the VAV air-conditioning system are shown in Table 2. The step response method is used to determine the delay time of the room temperature to the terminal air damper through experiments in summer and winter conditions.

During the experiment, the opening degree of the terminal air damper in the three rooms were the same. In order to ensure good indoor air distribution and air quality, the minimum air damper opening degree was 30%. Therefore, this article only studies the room temperature delay time of the terminal air damper adjustment when the air damper position changes between 30% and 100%. Fig. 10(a) shows the room temperature response curves of three rooms when the terminal air damper is adjusted under summer conditions. The air damper of the VAV junction box was maintained the minimum opening degree during 0–20 min. Manually adjust the air damper opening degree from 30% to 100% after 20 min. The temperature of three rooms dropped significantly at the 24th minute. Man-

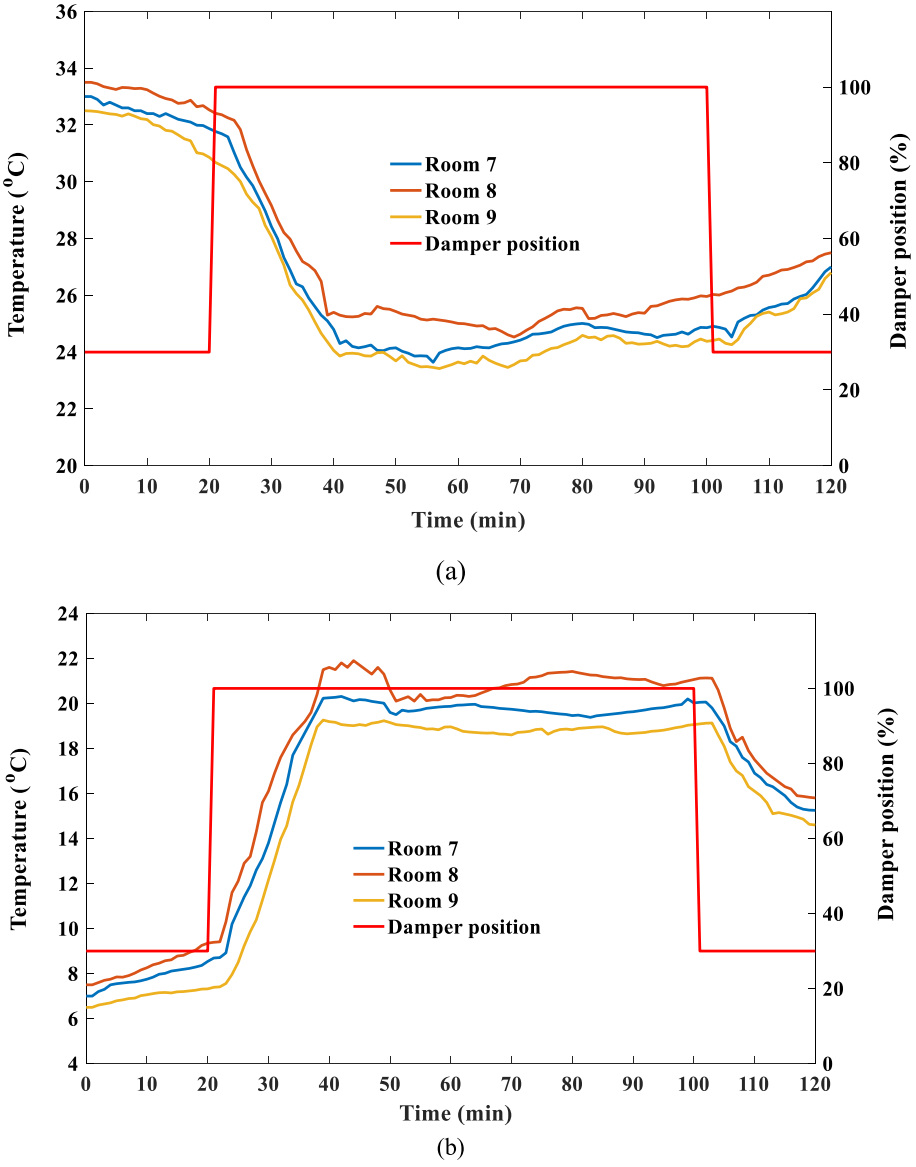

Fig. 10. Response curve of room temperature under (a) summer conditions and (b) winter conditions.

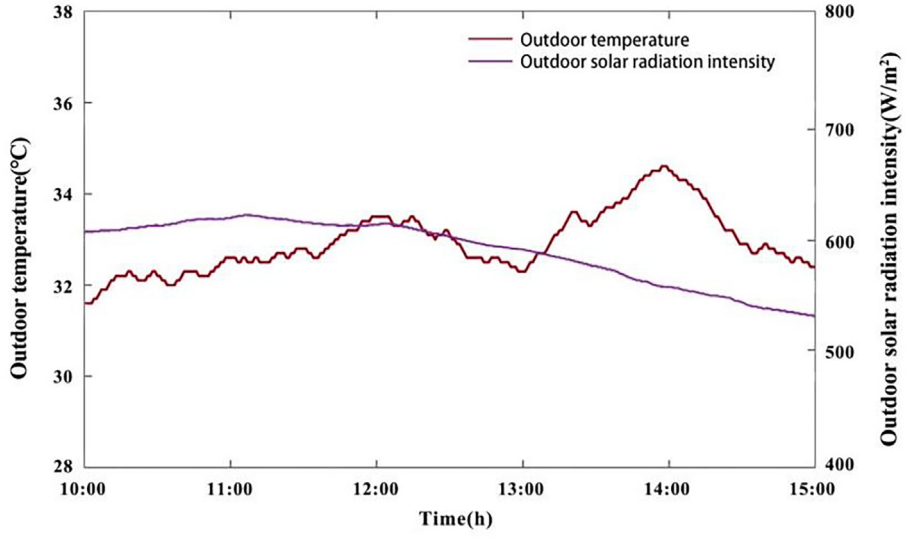

Fig. 11. Outdoor solar radiation intensity (W/m^2) and outdoor temperature (℃) in the control of outdoor environment using RBF NN predictive control model.

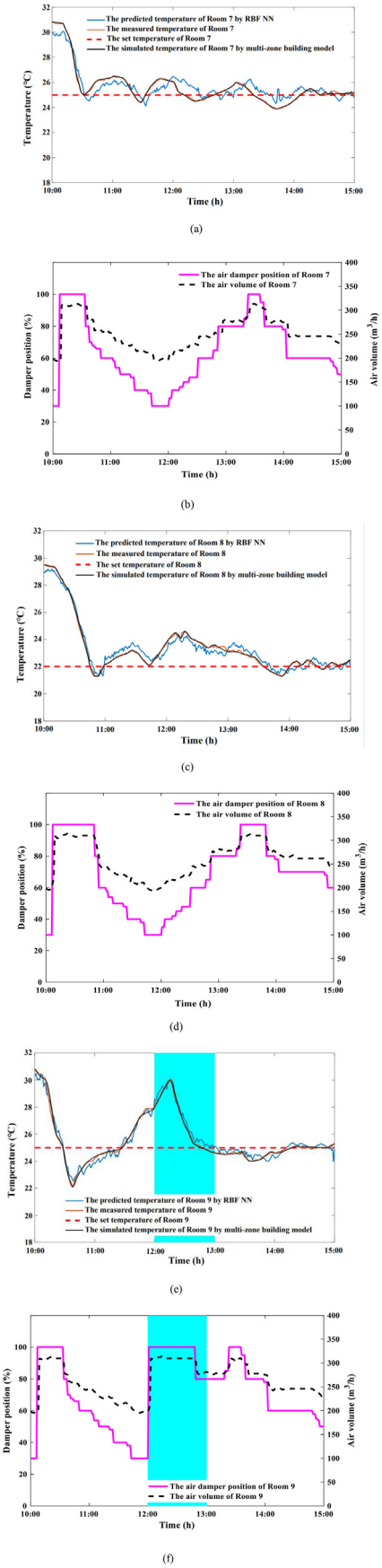

Fig. 12. Predictive control by RBF NN: (a) Room temperature control effect of Room 7, (b) The air volume and air damper position of Room 7, (c) Room temperature control effect of Room 8, (d) The air volume and air damper position of Room 8, (e) Room temperature control effect of Room 9, (f) The air volume and air damper position of Room 9.

ually adjust the air damper opening degree from 100% to 30% at the 100th minute. The temperature in three rooms rose at the 104th minute significantly. In winter and summer, the terminal air damper regulation is the same, and the room temperature response curves of three rooms under the terminal air damper regulation in winter are shown in Fig. 10 (b). The experiment showed that the room temperature decreased or increased significantly after the terminal air damper was adjusted for 4 min. Therefore, changing the opening degree of the terminal air damper has a certain delay on the change of room temperature, and the delay time is about 4 min.

4.2. Predictive control of multi-zone VAV air-conditioning system

In the multi-zone VAV air-conditioning system for Rooms 7, 8, and 9, the predictive control model is used to adjust the position of the terminal air damper continuously, so as to realize the periodical adjustment of the air supply volume and change the room temperature. The control period of VAV air-conditioning system is approximately equal to the delay response time of room temperature, that is, 4 min. This study uses Matlab software to load the RBF NN and Elman NN predictive algorithm into Simulink PLC Coder and then import the generated source file code to the SIMATIC S7-1200 programmable controller to realize the control.

In order to verify the accuracy of the room temperature dynamic response of the multi-zone building model when the air volume of each room is constantly changing, and ensure that the deviation between the predicted room temperature value and the room temperature set value output by the RBF NN under the condition of E that can be calculated by the PI algorithm, so that the air volume into the room can meet the demand. In the experiment, the indoor and outdoor environmental parameters are measured in real time, and the multi-zone building model will simulate the dynamic change of real-time temperature in each room. This experiment installs an electronic air flow measuring instrument FLY-1 in the VAV box of each room and records the air volume every minute. The supply air temperature is 16 °C. The indoor and outdoor temperature is measured every minute by self-recorder HOBO U23-001.The outdoor radiation intensity is measured by Solar Power Meter SM206. Fig. 11 shows outdoor solar radiation intensity (W/m^2) and outdoor temperature (℃). The measurements last for five hours.

The training of RBF NNs with different numbers of neurons in hidden layers is to determine the optimal structure. During the training, four neurons were first set in the hidden layer, and two more neurons were successively added after each training. The deviation E between the output of multi-zone building model and RBF NN model was taken as the criterion for stopping training of RBF NN. By comparing the results of multiple trainings, the RBF NN with 16 neurons in hidden layer was selected to predict indoor temperature, and the corresponding training time was 68.26 s.

The room temperature predictive control by RBF NN and the simulated indoor temperature change by multi-zone building model are shown in Fig. 12. The initial temperature of Rooms 7 and 8 are 30.8 °C and 29.5 °C respectively and the setpoints are 25 °C and 22 °C respectively as shown in Fig. 12(a) and Fig. 12(c). After 300 mins of operation and adjustment, the room temperature reaches the set value requirements. The indoor temperature of Room 7 reaches the set temperature for the first time in about 30 min. Due to the change of indoor and outdoor environment and the fluctuation of supply air static pressure of VAV air - conditioning, the ambient temperature is unstable and the fan speed changes, resulting in room temperature fluctuation. But the RBF NN has strong predictive performance, it can still accurately predict the change of the indoor temperature when the input parameters change. When the predictive control model based on the RBF NN outputs the optimal predictive value, according to the

deviation between the predicted value and the set value of room temperature, the opening degree of the air damper can be calculated by PI algorithm and adjusted regularly according to the control cycle, and the indoor air supply volume can be changed to adjust the room temperature. This control method can reduce the frequency and amplitude of the air damper and indoor temperature fluctuations, and make the room temperature fluctuations smaller. In order to verify the anti-interference ability of the RBF NN in the room temperature predictive control, the doors and windows of the Room 9 were opened from 12:00 to 13:00 to increase the heat load. The initial temperature of the Room 9 is 30.8℃, and the set temperature is 25℃ shown in Fig. 12(e). The room temperature suddenly increased during this period, and the input parameters were not adjusted in time. Therefore, the RBF NN has a certain error in predicting the room temperature in a short time in this process, but the RBF NN can make corresponding adjustments in time, accurately predict the room temperature, adjust the air damper opening degree in time, and change the indoor air supply volume. In the process of opening the doors and windows of the Room 9 to increase the heat load, the room temperature dropped rapidly at 12:20 and reached the set value at 12:45 for the first time. The process takes 45 min, and the frequency and amplitude of the room temperature fluctuation become smaller after reaching the set value. As shown in Fig. 12 (b), Fig. 12 (d), and Fig. 12 (f), the position of the air damper is adjusted by the RBF NN and the periodic predictive control model of the room temperature time-delay system of the multi-zone building model, and the fluctuation frequency of the air damper is relatively small. In this experiment, the simulated temperature using multi-zone building model agrees well with the measured temperature. It is proved again that the multi-zone building model established in this study can simulate the dynamic room temperature in real time and accurately.

In order to compare the control effect of the predictive control model established in this study and the Elman NN predictive control model on the terminal control of multi-zone VAV system under the same working conditions. The predictive control of the same multi-zone VAV air-conditioning system based on Elman NN is conducted. In order to ensure that the initial temperature of each room is the same as the initial temperature of each room in the above experiment, the air-conditioning system is used to adjust the indoor temperature of the three rooms before the experiment. The outdoor environment changes during the experiment are shown in Fig. 13.

The room temperature predicted by Elman NN and room temperature change simulated by multi-zone building model are shown in Fig. 14. The indoor temperature of room 7 also reached the set temperature for the first time in about 30 min as shown in Fig. 14 (a). Due to the change of indoor and outdoor environment and the fluctuation of supply air static pressure of VAV air-conditioning, the ambient temperature is unstable and the fan speed changes, resulting in room temperature fluctuation. This method can also predict room temperature changes as input parameters change. Fig. 14 (c) shows Room 8 reaching the set temperature in about 25 min. However, the error between the predicted value and the actual value is large, and the room temperature fluctuation is large. Fig. 14 (e) shows that during 12:00–13:00, all doors and windows in Room 9 are opened to increase the heat load. During this period, the room temperature dropped rapidly at 12:35 and reached the set value for the first time at 13:00. The process lasts 60 min. When the environment changes abruptly, the predictive control model fails to make corresponding adjustments in time, resulting in a large deviation between the room temperature and the set temperature. As shown in Fig. 14 (b), Fig. 14 (d), and Fig. 14 (f), the position of the air damper is adjusted by the Elman NN predictive control model, and the fluctuation frequency of the air damper is relatively large. It shows that the predictive control model in this study is more stable and faster than the Elman NN predictive control model in predicting the room temperature effect.

By quantitative analysis on the experimental results in Fig. 12 and Fig. 14. The average differences between the room temperature predicted by the model and the measured temperature of the Room 7, Room 8 and Room 9 are 0.31 °C, 0.35 °C and 0.38 °C, respectively. With the Elman NN model, the average difference between the predicted room temperature and the measured value of Room 7, Room 8 and Room 9 is 0.42 °C, 0.66 °C and 0.68 °C, respectively. For example, in room 8, the predicted room temperature by Elman NN model and the setpoint deviate greatly. The opening degree of the air damper and the air supply volume fluctuates greatly. The predicted value and the setpoint of room temperature are similar. The air damper opening degree and the air supply volume has little fluctuation and is more stable. The similar phenomenon would be observed in the results of other rooms.

The air volume sent into the room by the terminal equipment of the VAV air-conditioning system can meet the air volume demand of the room, and the influence of the pressure change in the air

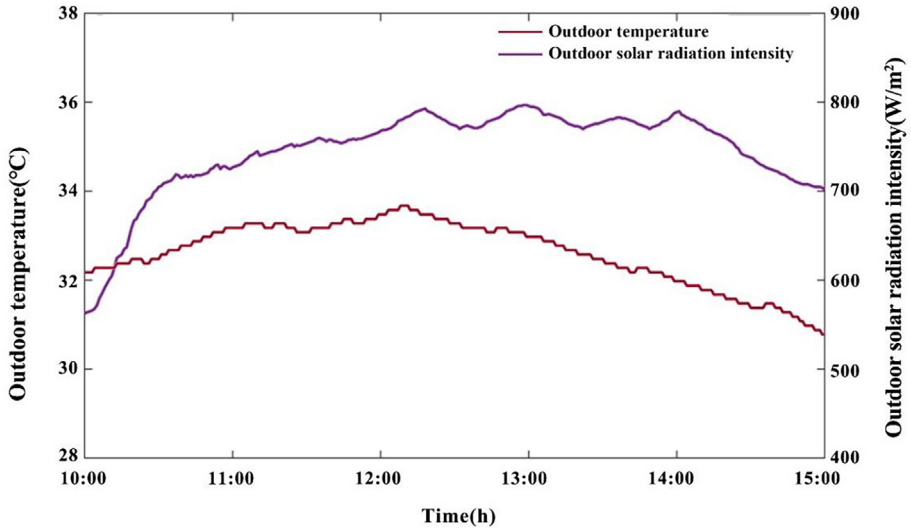

Fig. 13. Outdoor solar radiation intensity (W/m^2) and outdoor temperature (℃) in the control of outdoor environment using Elman NN predictive control model.

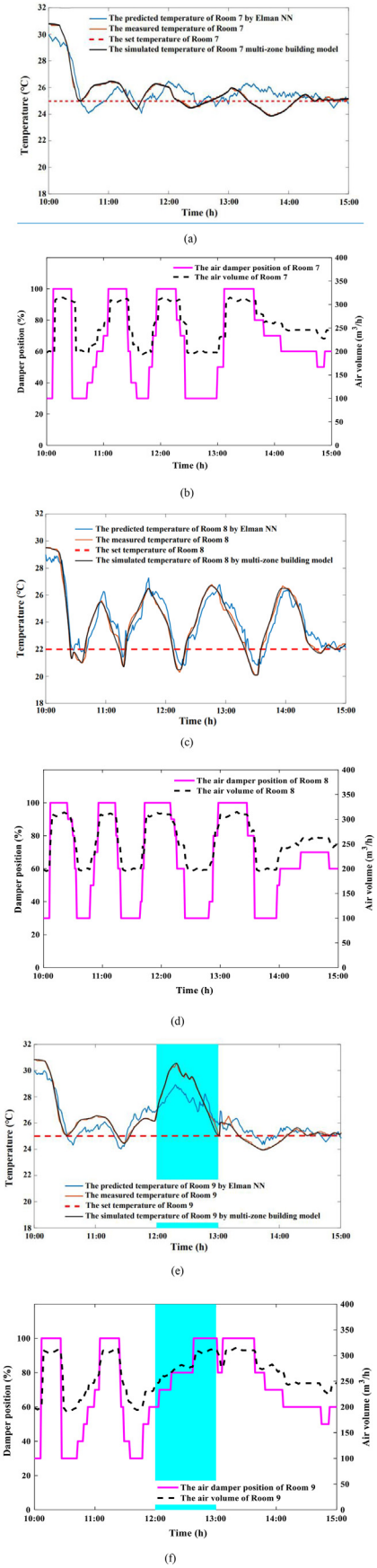

Fig. 14. Predictive control effect based on Elman NN: (a) Room temperature control effect of Room 7, (b) The air volume and air damper position of Room 7, (c) Room temperature control effect of Room 8, (d) The air volume and air damper position of Room 8, (e) Room temperature control effect of Room 9, (f) The air volume and air damper position of Room 9.

supply pipe on the experimental control effect is reduced. The static pressure control method is adopted in the experiment. The WH131 static pressure sensor is installed in the middle of the main air supply duct between rooms 8 and 9. The static pressure of the supply air is set to 60 Pa. As shown in Fig. 15, with the control by RBF NN, although the static pressure of the supply air fluctuates with little amplitude. However, the predictive control by the Elman NN has greater fluctuations in the static pressure of the air supply compared with that of the RBF NN. When the predictive control model based on the RBF NN and multi-zone building model is used, the average deviation between the supply air static pressure and the set value is 2.01 Pa. While the Elman NN predictive control model is used, the average deviation between the supply air static pressure and the set value is 8.25 Pa. The comparisons further confirm that the control by RBF NN is more stable.

5. Conclusions

In order to establish a multi-zone building model that can simulate real-time changes of room temperature based on air volume changes, building envelope and indoor and outdoor environmental parameters, this research proposes the RC network two-node wall structure method. This method first divides building envelope such as walls and floors into two-story structures, and then uses energy balance theory to establish the energy balance equation of each node. Finally, the dynamic response equations of room temperature and humidity in each room of the whole building are obtained. At the same time, a periodic predictive control model of time-delay system at room temperature based on RBF NN and multi-zone building model is proposed. This model can accurately predict and control room temperature according to the variation of air volume, building envelope and indoor and outdoor environmental parameters, and experiments are carried out in the control of multi-zone VAV air-conditioning system. The following conclusions are obtained:

(1) The multi-zone building model based on RC network two-node wall structure method can accurately simulate the dynamic change of room temperature.
(2) When the room setpoint temperature is low, the periodic predictive control model of time-delay systems at room temperature based on RBF NN and multi-zone building model avoids the large fluctuation of the air damper and improves the stability of room temperature.
(3) The periodic predictive control model has strong anti-interference ability. It ensures stable static pressure of the main air supply duct of the multi-zone VAV air-conditioning system.

Declaration of Competing Interest

The authors declare that they have no known competing financial interests or personal relationships that could have appeared to influence the work reported in this paper.

Acknowledgments

This research was supported by the National Natural Science Foundation of China (Grant No.: 51708146 and 51808487). Wei Liu acknowledges financial support from Stiftelsen för internationalisering av högre utbild-ning och forskning (STINT), Sweden (Dnr: CH2020-8665)

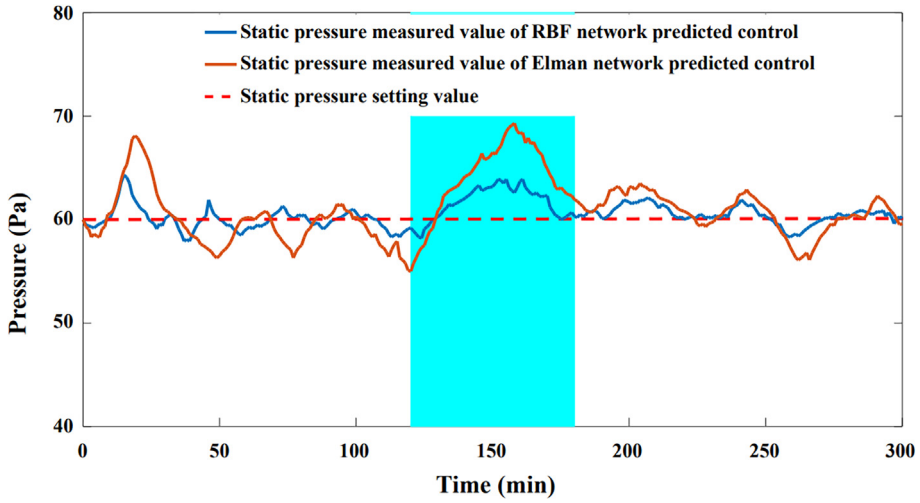

Fig. 15. Static pressure of main air supply duct.

Appendix A. . The expression form of correlation coefficients in Eq. (23)

A, B and C are correlation coefficients of X ,U and $\frac{dX}{dt}$ in Eq. (23) respectively.

(1) The expression form of A is shown as follows:

$$A=\begin{bmatrix} A1 & \frac{4K_{wa,in}A_{wa,w}K_{wa}}{4K_{wa}+K_{wa,in}} & 0 & \frac{4K_{fl}A_{fl,w}K_{fl,in}}{4K_{fl}+K_{fl,in}} & 0 & 0 \\ 0 & \frac{4A_{wa}K_{wa}}{1+\frac{K_{wa,in}}{4K_{wa}}}-6K_{wa}A_{wa} & 2A_{wa}K_{wa} & 0 & 0 & 0 \\ 0 & 2A_{wa}K_{wa} & \frac{4A_{wa}K_{wa}}{1+\frac{K_{wa,in}}{4K_{wa}}}-6A_{wa}K_{wa} & 0 & 0 & 0 \\ 0 & 0 & 0 & \frac{4A_{fl}K_{fl}}{1+\frac{K_{fl,in}}{4K_{fl}}}-6A_{fl}K_{fl} & 2A_{fl}K_{fl} & 0 \\ 0 & 0 & 0 & 2A_{fl}K_{fl} & \frac{4A_{fl}K_{fl}}{1+\frac{K_{fl,out}}{4K_{fl}}}-6A_{fl}K_{fl} & 0 \\ 0 & \frac{4K_{wa,in}A_{wa,s}K_{wa}}{4K_{wa}+K_{wa,in}} & 0 & \frac{4K_{fl,in}A_{fl,s}K_{fl}}{4K_{fl}+K_{fl,in}} & 0 & -G_{sa,sw}-\sum_i \rho_a V_{adj}C_aR \\ 0 & \frac{4K_{wa,in}A_{wa,r}K_{wa}}{4K_{wa}+K_{wa,in}} & 0 & 0 & 0 & 0 \\ 0 & 0 & 0 & 0 & 0 & 0 \\ 0 & 0 & 0 & 0 & 0 & 0 \end{bmatrix}$$

$$\begin{bmatrix} \frac{K_{fl,in}A_{fl,w}K_{fl,in}}{4K_{fl}+K_{fl,in}} & \frac{K_{wa,in}A_{wa,w}K_{wa,in}}{4K_{wa}+K_{wa,in}} & 0 & 0 \\ 0 & \frac{4A_{wa}K_{wa}}{1+4\frac{K_{wa}}{K_{wa,in}}} & 0 & 0 \\ 0 & 0 & 0 & 0 \\ \frac{4A_{fl}K_{fl}}{1+4\frac{K_{fl}}{K_{gl,in}}} & 0 & 0 & 0 \\ 0 & 0 & 0 & 0 \\ 0 & 0 & G_{sa,sw} & 0 \\ \frac{K_{fl,in}A_{fl,s}K_{fl,in}}{4K_{fl}+K_{fl,in}}-K_{wa,in}A_{wa,s}-K_{fl,in}A_{fl,s}-G_{sa}C_a & \frac{K_{wa,in}A_{wa,s}K_{wa,in}}{4K_{wa}+K_{wa,in}} & 0 & 0 \\ G_{sa,sr}C_a & \frac{K_{wa,in}A_{wa,r}K_{wa,in}}{4K_{wa}+K_{wa,in}}-K_{wa,in}A_{wa,r}-G_{sa,sr}C_a-G_{sa,sw}C_a & 0 & 0 \\ 0 & 0 & -G_{sa} & 0 \\ 0 & 0 & G_{sa,sr} & -G_{sa,sw}-G_{sa,sr} \end{bmatrix}$$

Among them:

$$A1=-K_{wa,in}A_{wa,s}-K_{win}A_{win}-K_{fl,in}A_{fl,s}-G_{sa}C_a-\sum_i \rho_a V_{adj,i}C_aR - A_{la}K_{la}$$

(2) The expression form of B is shown as follows:

$$B=\begin{bmatrix} K_{win}A_{win} & T_{sa}V_{sa}C_a & A_{la}K_{la} & \sum_i \rho_a V_{adj,i}C_aR & 0 \\ 0 & 0 & 0 & 0 & 0 \\ \frac{4A_{wa}K_{wa}}{1+4\frac{K_{wa}}{K_{wa,out}}} & 0 & 0 & 0 & 0 \\ 0 & 0 & 0 & 0 & 0 \\ \frac{4A_{fl}K_{fl}}{1+4\frac{K_{fl}}{K_{fl,out}}} & 0 & 0 & 0 & 0 \\ 0 & 0 & 0 & 0 & \sum_i \rho_a V_{adj}C_aR \\ 0 & C_aT_{sa} & 0 & 0 & 0 \\ 0 & 0 & 0 & 0 & 0 \\ 0 & M_{sa} & 0 & 0 & 0 \\ 0 & 0 & 0 & 0 & 0 \end{bmatrix}$$

(3) The expression form of C is shown as follows:

$$C = \begin{bmatrix} \rho_a V C_a & 0 & 0 & 0 & 0 & 0 & 0 & 0 & 0 & 0 \\ 0 & \frac{\rho_{wa}\delta_{wa}A_{wa}C_{wa}}{2} & 0 & 0 & 0 & 0 & 0 & 0 & 0 & 0 \\ 0 & 0 & \frac{\rho_{wa}\delta_{wa}A_{wa}C_{wa}}{2} & 0 & 0 & 0 & 0 & 0 & 0 & 0 \\ 0 & 0 & 0 & \frac{\rho_{fl}\delta_{fl}A_{fl}C_{fl}}{2} & 0 & 0 & 0 & 0 & 0 & 0 \\ 0 & 0 & 0 & 0 & \frac{\rho_{fl}\delta_{fl}A_{fl}C_{fl}}{2} & 0 & 0 & 0 & 0 & 0 \\ 0 & 0 & 0 & 0 & 0 & V_{in}\rho_a & 0 & 0 & 0 & 0 \\ 0 & 0 & 0 & 0 & 0 & 0 & V_{ins}\rho_a C_a & 0 & 0 & 0 \\ 0 & 0 & 0 & 0 & 0 & 0 & 0 & V_{inr}\rho_a C_a & 0 & 0 \\ 0 & 0 & 0 & 0 & 0 & 0 & 0 & 0 & V_{ins}\rho_a & 0 \\ 0 & 0 & 0 & 0 & 0 & 0 & 0 & 0 & 0 & V_{inr}\rho_a \end{bmatrix}$$

where the expression form of C^- is shown as follows:

$$C^{-} = \begin{bmatrix} \frac{1}{\rho_a V C_a} & 0 & 0 & 0 & 0 & 0 & 0 & 0 & 0 & 0 \\ 0 & \frac{2}{\rho_{wa}\delta_{wa}A_{wa}C_{wa}} & 0 & 0 & 0 & 0 & 0 & 0 & 0 & 0 \\ 0 & 0 & \frac{2}{\rho_{wa}\delta_{wa}A_{wa}C_{wa}} & 0 & 0 & 0 & 0 & 0 & 0 & 0 \\ 0 & 0 & 0 & \frac{2}{\rho_{fl}\delta_{fl}A_{fl}C_{fl}} & 0 & 0 & 0 & 0 & 0 & 0 \\ 0 & 0 & 0 & 0 & \frac{2}{\rho_{fl}\delta_{fl}A_{fl}C_{fl}} & 0 & 0 & 0 & 0 & 0 \\ 0 & 0 & 0 & 0 & 0 & \frac{1}{V_{in}\rho_a} & 0 & 0 & 0 & 0 \\ 0 & 0 & 0 & 0 & 0 & 0 & \frac{1}{V_{ins}\rho_a C_a} & 0 & 0 & 0 \\ 0 & 0 & 0 & 0 & 0 & 0 & 0 & \frac{1}{V_{inr}\rho_a C_a} & 0 & 0 \\ 0 & 0 & 0 & 0 & 0 & 0 & 0 & 0 & \frac{1}{V_{ins}\rho_a} & 0 \\ 0 & 0 & 0 & 0 & 0 & 0 & 0 & 0 & 0 & \frac{1}{V_{inr}\rho_a} \end{bmatrix}$$

References

[1] X. Xu, S. Wang, Z. Sun, F.u. Xiao, A model-based optimal ventilation control strategy of multi-zone VAV air-conditioning systems, Appl. Thermal Eng. 29 (1) (2009) 91–104.

[2] Y.e. Yao, Z. Lian, W. Liu, Z. Hou, M. Wu, Evaluation program for the energy-saving of variable-air-volume systems, Energy and Buildings. 39 (5) (2007) 558–568.

[3] S.A. Mumma, R.J. Bolin, Energy optimized-ventilation constrained variable air volume system control, Automation in Construction. 6 (5-6) (1997) 463–470.

[4] H. Ion, G. Christian, P. David, Optimal temperature control of intermittently heated buildings using model predictive control: part II e control algorithm, Building and Environment 51 (2012) 388–394.

[5] Z.-M. Yi, H. Yu, Q.i. Wei, X.-Y. Chu, An advanced simulation test bed for the stability analysis of variable air volume air-conditioning control system. Part 1: Optimal simplified model of building envelope for room thermal performance prediction, Energy and Buildings. 158 (2018) 950–963.

[6] Z. Wang, Y. Chen, Y. Li, Development of RC model for thermal dynamic analysis of buildings through model structure simplification, Energy and Buildings. 195 (2019) 51–67.

[7] X. Jin, S. Wang, A multi-area building model for control analysis of air conditioning systems, Fluid Machinery. 27 (3) (1999) 45–50.

[8] S.-H. Kang, H.-J. Kim, Y.-H. Cho, A study on the control method of single duct VAV terminal unit through the determination of proper minimum air flow, Energy and Buildings. 69 (2014) 464–472.

[9] T.I. Salsbury, A temperature controller for VAV air-handling units based on simplified physical models, HVAC&R Res. 4 (3) (1998) 265–279.

[10] X. Li, S. Lin, J. Zhang, T. Zhao, Model parameter identification of indoor temperature lag characteristic based on hysteresis relay feedback control in VAV systems, J. Build. Eng. 25 (2019) 100839, https://doi.org/10.1016/j.jobe.2019.100839.

[11] X. Li, Z. Han, T. Zhao, J. Gao, Online model for indoor temperature control based on building thermal process of air conditioning system, J. Build. Eng. 39 (2021) 102270, https://doi.org/10.1016/j.jobe.2021.102270.

[12] T. Xing, X. Li, J. Zhang, An identification method for room temperature dynamic model based on analytical solution in VAV system, Energy and Buildings. 174 (2018) 134–146.

[13] S. Goyal, P. Barooah, A method for model-reduction of non-linear thermal dynamics of multi-zone buildings, Energy and Buildings. 47 (2012) 332–340.

[14] E. Atam, Decentralized thermal modeling of multi-zone buildings for control applications and investigation of submodeling error propagation, Energy and Buildings. 126 (2016) 384–395.

[15] J. Bai, S. Wang, X. Zhang, Development of an adaptive Smith predictor-based self-tuning PI controller for an HVAC system in an experiment room, Energy and Buildings. 40 (2008) 2244–2252.

[16] M. Xu, S. Li, Practical generalized predictive control with decentralized identification approach to HVAC systems, Energy Conversion and Management. 48 (1) (2007) 292–299.

[17] J. Zhang, X. Li, T. Zhao, W. Dai, Experimental study on a novel fuzzy control method for static pressure reset based on the maximum damper position feedback, Energy and Buildings. 108 (2015) 215–222.

[18] T. Lu, M. Viljanen, Prediction of indoor temperature and relative humidity using neural network models: model comparison, Neural Computing & Applications. 18 (4) (2009) 345–357.

[19] A. Kusiak, G. Xu, Modeling and optimization of HVAC systems using a dynamic neural network, Energy. 42 (1) (2012) 241–250.

[20] H. Huang, L. Chen, E. Hu, A neural network-based multi-zone modelling approach for predictive control system design in commercial buildings, Energy and Buildings. 97 (2015) 86–97.

[21] X. Li, T. Zhao, J. Zhang, T. Chen, Predication control for indoor temperature time-delay using Elman neural network in variable air volume system, Energy and Buildings. 154 (2017) 545–552.

[22] X. Li, Z. Han, T. Zhao, J. Zhang, D.a. Xue, Modeling for indoor temperature prediction based on time-delay and Elman neural network in air conditioning system, J. Build. Eng. 33 (2021) 101854, https://doi.org/10.1016/j.jobe.2020.101854.

[23] G. Huang, Model predictive control of VAV zone thermal systems concerning bi-linearity and gain nonlinearity, Control Eng. Practice. 19 (7) (2011) 700–710.

[24] Y. Wang, Y. Shi, M. Cai, W. Xu, Predictive control of air-fuel ratio in aircraft engine on fuel-powered unmanned aerial vehicle using fuzzy-RBF neural network, J. Franklin Institute. 357 (13) (2020) 8342–8363.

[25] Y. Deng, X. Zhou, J. Shen, G.e. Xiao, H. Hong, H. Lin, F. Wu, B.-Q. Liao, New methods based on back propagation (BP) and radial basis function (RBF)

artificial neural networks (ANNs) for predicting the occurrence of haloketones in tap water, Sci. Total Environ. 772 (2021) 145534, https://doi.org/10.1016/j.scitotenv.2021.145534.
[26] S. Han, H. Wang, Y. Tian, N. Christov, Time-delay estimation based computed torque control with robust adaptive RBF neural network compensator for a rehabilitation exoskeleton, ISA Transactions. 97 (2019) 172–181.
[27] H. Hamdi, C. Ben Regaya, A. Zaafouri, Real-time study of a photovoltaic system with boost converter using the PSO-RBF neural network algorithms in a MyRio controller, Solar Energy. 183 (2019) 1–16.
[28] F. Girosi, T. Poggio, Networks and the best approximation property, Biological Cybernetics. 63 (3) (1990) 169–176.
[29] Y.e. Yao, Z. Lian, Z. Hou, W. Liu, An innovative air-conditioning load forecasting model based on RBF neural network and combined residual error correction, Int. J. Refrig. 29 (4) (2006) 528–538.
[30] S. Faizollahzadeh Ardabili, A. Mahmoudi, T. Mesri Gundoshmian, Modeling and simulation controlling system of HVAC using fuzzy and predictive (radial basis function, RBF) controllers, J. Build. Eng. 6 (2016) 301–308.
[31] S. Zheng, X. Huang, S. Tang, N. Zhao, R. Ma, K. Chang, Indoor air conditioning temperature control system based on RBF fuzzy PID control algorithm, AISI 2021 (100) (2021) 247–255.